Hydrodynamic Lyapunov modes in coupled map lattices

Hong-liu Yang* and Günter Radons†
Institute of Physics, Chemnitz University of Technology, D-09107 Chemnitz, Germany
(Received 8 July 2005; published 4 January 2006)

In this paper, numerical and analytical results are presented which indicate that hydrodynamic Lyapunov modes (HLMs) also exist for coupled map lattices (CMLs). The dispersion relations for the HLMs of CMLs are found to fall into two different universality classes. It is characterized by $\lambda \sim k$ for coupled standard maps and $\lambda \sim k^2$ for coupled circle maps. The conditions under which HLMs can be observed are discussed. The role of the Hamiltonian structure, conservation laws, translational invariance, and damping is elaborated. Our results are as follows: (1) The Hamiltonian structure is not a necessary condition for the existence of HLMs. (2) Conservation laws or the translational invariance alone cannot guarantee the existence of HLMs. (3) Including a damping term in the system of coupled Hamiltonian maps does not destroy the HLMs. The λ-k dispersion relation of HLMs, however, changes to the universality class with $\lambda \sim k^2$ under damping. In contrast, no HLMs survives in the system of coupled circle maps under damping. (4) An on-site potential destroys the HLMs. (5) The study of zero-value Lyapunov exponents (LEs) and associated Lyapunov vectors (LVs) shows that translational invariance and conservation laws play different roles in the tangent space dynamics. (6) The dynamics of the coordinate and momentum parts of LVs in Hamiltonian systems are related but different. Furthermore, numerical results for a two-dimensional system show that the appearance of HLMs in CMLs is not restricted to the one-dimensional case.

DOI: 10.1103/PhysRevE.73.016202 PACS number(s): 05.45.Jn, 05.10.−a, 05.20.−y, 05.20.Jj

I. INTRODUCTION

The study of nonlinear systems with many degrees of freedoms is of importance in understanding the fundamental problems of nonequilibrium statistical mechanics on the basis of the modern theory of chaotic dynamics [1]. In the past decade, some beautiful theories in this direction were developed [2–6]. For instance, quantities characterizing the dynamical randomness of a nonlinear system, such as the Kolmogorov-Sinai entropy and Lyapunov exponents, were connected to certain transport coefficients.

In contrast to this success, there is little progress in understanding the information contained in Lyapunov vectors (LVs). An exception is the recent discovery of *hydrodynamic Lyapunov modes* (HLMs) by Posch *et al.* in molecular dynamics simulations of hard-ball systems [7]. HLMs are regular collective perturbations corresponding to the smallest positive Lyapunov exponents of a many-degree-of-freedom system, i.e., they are slow modes characterizing in some respects the global structure of high-dimensional systems. This nature makes them important for a coarse-grained reduced description of high-dimensional nonlinear systems. It is expected that there is a connection between these modes and the macroscopic properties of such systems. Moreover, the study of this interesting phenomenon has its own importance in understanding the universal features of high-dimensional nonlinear systems. Two kinds of modes were found by Posch *et al.* in simulations of two-dimensional hard-disk systems. They found transverse hydrodynamic Lyapunov modes, which are stationary and longitudinal modes which are propagating.

Since this discovery, a lot of work has been done in order to uncover the underlying mechanisms and to elaborate the properties of HLMs [7–18]. Until now, however, no satisfactory explanation has been offered and even the question when and where these modes may appear remains a mystery. In spite of this, it is generally believed that conservation laws and/or continuous symmetries should play an essential role. Eckmann and Gat [10] used a random matrix approximation to prove the existence of hydrodynamic Lyapunov modes in translational invariant systems with uniform hyperbolicity. McNamara and Mareschal [11] proposed a generalized hydrodynamic theory which can properly predict the appearance of two kinds of hydrodynamic Lyapunov modes. De Wijn and van Beijeren [12] suggested an alternative point of view in terms of Goldstone modes. In simulations of quasi-one-dimensional hard-disk systems with different boundary conditions, Taniguchi and Morriss found that there is a new kind of momentum-proportional hydrodynamic Lyapunov modes besides the stationary transverse modes and the propagating longitudinal modes [13]. In a recent work, Eckmann *et al.* classify all the modes in hard-core systems into three groups as transverse, longitudinal, and P modes, respectively [14]. They conjectured that the longitudinal and P modes are contained in the longitudinal branch and form so-called LP pairs. It was further shown that the observed propagation of the modes is due to a rotation of the LP pair in the subspace spanned by them. Our work on Lennard-Jones fluids provided numerical evidence for the existence of hydrodynamic Lyapunov modes in systems with soft-potential interaction [15]. We proposed a description of Lyapunov vectors in analogy to the correlation function theory of fluctuations in fluids [16]. This provided a quantitative measure characterizing the spatial structure and the dynamics of Lyapunov vectors in extended systems and made the classification of hydrodynamic Lyapunov modes

*Electronic address: hongliu.yang@physik.tu-chemnitz.de
†Electronic address: radons@physik.tu-chemnitz.de

unambiguous. The finding of HLMs in soft-potential systems was later confirmed by work of Forster and Posch on WCA fluids [17].

In this paper we use simple model systems of coupled map lattices (CMLs) to perform a series of numerical experiments and try to shed some light on the conditions under which hydrodynamic Lyapunov modes can be observed. Coupled map lattices provide dynamical systems which are discrete in space and time while continuous in state space. They were originally invented by K. Kaneko in the study of spatio-temporal chaos [19]. During the past decades these simple model systems attracted a lot of interest in various fields such as spatio-temporal chaos and pattern formation, neural networks, biochemical reactions, and secure communication [20,21]. In the study of the Lyapunov instability of CMLs, it was found that the Lyapunov spectrum tends to be a smooth curve as the thermodynamic limit is approached gradually [22]. In addition the Lyapunov vector associated with the largest Lyapunov exponent was found to be localized in space [23–25]. The selection of this popular and convenient paradigm as subject of the current study has a twofold motivation. The use of such a model will, on one hand, allow us to check the generality and universality of hydrodynamic Lyapunov modes found in many-particle systems. Although the CMLs cannot be directly related to the many-particle systems investigated previously, they do bear similar symmetries, which are intuitively expected to be an essential ingredient for the existence of HLMs. On the other hand, CMLs are easy to simulate and can be tuned flexibly. This is crucial for our design of controllable experiments to analyze the role played by different factors.

We start in Sec. II with a short description of the correlation function theory for Lyapunov vectors. In the study of Lennard-Jones fluids, the method was shown to be powerful in detecting and characterizing the otherwise difficult to observe hydrodynamic Lyapunov modes. Here we rely on this tool again in the study of CMLs. The results shown here are mainly on the spatial structure of the Lyapunov vectors. The dynamical properties of the LVs will be presented elsewhere [26]. In Sec. III, numerical results are presented to show that the HLMs do exist for coupled standard maps. In Secs. IV–VIII, the role of Hamiltonian structure, conservation laws and translational invariance, damping, and an on-site potential is investigated. Section IX is devoted to the study of the universality of the λ-k dispersion relation of HLMs. The relation between the coordinate and momentum part of LVs of Hamiltonian systems is investigated in Sec. X. A close view of the zero-value LEs and the corresponding LVs is reported in Sec. XI. Section XII briefly treats HLMs in a two-dimensional lattice of coupled maps. The paper closes with a summary of the results and a discussion.

II. CORRELATION FUNCTIONS FOR LYAPUNOV VECTORS

In previous studies of hydrodynamic Lyapunov modes the identification of modes relied mainly on the naked eye to find the wave-like structures and the extraction of the mode parameters is based on the direct numerical fitting of the time-averaged Lyapunov vector to a sinusoidal function. Although this way is straightforward and has been successful in studies of hard-ball systems, an unambiguous identification of vague or mixing modes is very difficult. For the nonstationary modes, the extracted characterizing parameters become quite inaccurate since time averaging can no longer be used to suppress noise here. These drawbacks of the direct numerical fitting call for a more accurate method to identify the modes and to characterize their dynamics.

In the study of Lennard-Jones fluids, the correlation function method for Lyapunov vectors was developed and tested [15,16]. It was shown to be powerful in classifying and characterizing the vague hydrodynamic Lyapunov modes. A brief description of the method is recalled here.

In analogy to the definition of other microscopic densities in the theory of liquids [27], we introduce a dynamical variable called *LV fluctuation density*

$$\mathcal{U}^{(\alpha)}(r,t) = \sum_{l=1}^{L} \delta u_l^{(\alpha)}(t)\,\delta(r - r_l(t)), \tag{1}$$

where $\delta(x)$ is Dirac's delta function, $r_l(t)$ is the position coordinate of the lth element, and $\{\delta u_l^{(\alpha)}(t)\}$ is the coordinate part of the αth Lyapunov vector $\mathbf{f}^{(\alpha)}$ [28,29].

Recall that in the seminal work about the multiplicative ergodic theorem Oseledec proved that the limit $\Xi = \lim_{t\to+\infty}[M^T(t,0)\cdot M(t,0)]^{1/2t}$ exists for almost every initial point of a nonlinear dynamical system, where $M(t,0)$ is the fundamental matrix governing the time evolution of perturbations $\delta X(t)$ in tangent space as $\delta X(t) = M(t,0)\cdot\delta X(0)$ [2]. This provides a firm mathematical basis for the existence of the Lyapunov exponents and Lyapunov vectors in multidimensional nonlinear systems. The set of Lyapunov exponents is defined as $\lambda^{(\alpha)} = \ln \mu^{(\alpha)}$, where $\mu^{(\alpha)}$ are the eigenvalues of the matrix Ξ, i.e., $\Xi\cdot\mathbf{g}^{(\alpha)} = \mu^{(\alpha)}\mathbf{g}^{(\alpha)}$. In practice the Lyapunov exponents are calculated via the so-called standard method invented by Benettin and Shimada *et al.* [33,34], which is also used in the current paper. Here the time evolution of a set of offset vectors in tangent space is monitored by integrating the linearized equation. And the offset vectors are reorthonormalized periodically. The time-averaged values of the logarithms of the renormalization factors are the Lyapunov exponents and the set of offset vectors $\mathbf{f}^{(\alpha)}$ right after the reorthonormalization are the Lyapunov vectors. The equivalence of the Lyapunov exponents obtained via the two methods is quite obvious and a rigorous proof can be found in Ref. [30]. The relation between the Oseledec eigenvectors $\mathbf{g}^{(\alpha)}$ and the Lyapunov vectors obtained via the standard method is more subtle. It is proved that the Lyapunov vectors $\mathbf{f}^{(\alpha)}$ obtained via the standard method converge exponentially to the Oseledec eigenvectors for the inverse-time dynamics of the original system. In other words, as $t\to+\infty$, there is $\mathbf{f}^{(\alpha)} \sim \mathbf{g}^{(\alpha)}$, where $\mathbf{g}^{(\alpha)}$ are eigenvectors of the matrix $\bar{\Xi} = \lim_{t\to+\infty}[\overline{M(t,0)}^T\cdot\overline{M(t,0)}]^{1/2t}$ as well as its inverse $\bar{\Xi}^{-1} = \lim_{t\to+\infty}[M(t,0)\cdot M(t,0)^T]^{1/2t}$ and $\overline{M(t,0)} \equiv [M(t,0)]^{-1}$ is the fundamental matrix of the inverse-time dynamics. See Refs. [31,32] for the details.

A space- and time-dependent autocorrelation function of the LV fluctuation density akin to the van Hove correlation function is defined

$$G_u^{(\alpha\alpha)}(r,t) = \langle \mathcal{U}^{(\alpha)}(r,t)\mathcal{U}^{(\alpha)}(0,0)\rangle. \quad (2)$$

The structural features of the Lyapunov vectors are captured by the spatial Fourier transformation of the equal time correlation function $G_u^{(\alpha\alpha)}(r,0)$:

$$S_u^{(\alpha\alpha)}(k) = \int G_u^{(\alpha\alpha)}(r,0)e^{-jk\cdot r}dr. \quad (3)$$

We call it the *static LV structure factor*. By introducing the spatial Fourier transformation of $\mathcal{U}^{(\alpha)}(r,t)$

$$\mathcal{U}_k^{(\alpha)}(t) = \int \mathcal{U}^{(\alpha)}(r,t)e^{-jk\cdot r}dr = \sum_{l=1}^{L} \delta u_l^{(\alpha)}(t)e^{-jk\cdot r_l(t)} \quad (4)$$

and the correlation function of $\mathcal{U}_k^{(\alpha)}(t)$

$$F_u^{(\alpha\alpha)}(k,t) = \langle \mathcal{U}_k^{(\alpha)}(t)\mathcal{U}_{-k}^{(\alpha)}(0)\rangle = \int G_u^{(\alpha\alpha)}(r,t)e^{-jk\cdot r}dr \quad (5)$$

it is easy to see that

$$S_u^{(\alpha\alpha)}(k) = F_u^{(\alpha\alpha)}(k,0), \quad (6)$$

i.e., the static LV structure factor is nothing but the spatial power spectrum of the LV fluctuation density $\mathcal{U}^{(\alpha)}(r,t)$. The spectrum of $F_u^{(\alpha\alpha)}(k,t)$, defined as

$$S_u^{(\alpha\alpha)}(k,\omega) = \int F_u^{(\alpha\alpha)}(k,t)e^{j\omega t}dt, \quad (7)$$

which encodes additional information on the dynamics of the LVs, is called the *dynamic LV structure factor*.

In many-particle systems the space translational invariance yields Lyapunov vectors with constant coordinate part $\delta u_l^{(\alpha)} = c^{(\alpha)}$ corresponding to certain zero-value Lyapunov exponents. For these special cases the LV density variable $\mathcal{U}^{(\alpha_0)}(r,t)$ is proportional to the ordinary microscopic particle density $\mathcal{U}^{(\alpha_0)}(r,t) = c^{(\alpha_0)}\rho(r,t)$ with $\rho(r,t) = \Sigma_{l=1}^{L}\delta(r - r_l(t))$. Corresponding for these zero modes the components of the LV density correlation function $S_u^{(\alpha_0\alpha_0)}(k)$ and $S_u^{(\alpha_0\alpha_0)}(k,w)$ are simply proportional to the static and dynamic structure factor $S(k)$ and $S(k,\omega)$, respectively.

In general, $\mathcal{U}^{(\alpha)}(r,t)$ is a vector field and the correlation function $F_u^{(\alpha\alpha)}(k,t)$ is a second rank tensor [16]. For isotropic systems the correlation tensor has only two independent components, implying that these two terms correspond to the transverse and longitudinal hydrodynamic Lyapunov modes, respectively. This was confirmed in numerical simulations for Lennard-Jones fluids [16].

III. HYDRODYNAMIC LYAPUNOV MODES IN LATTICE OF HAMILTONIAN MAPS

The first model we investigated is a lattice of Hamiltonian maps with a force-like coupling [35]. It is of the form

$$v_{t+1}^l = (1 - \gamma_t^l)v_t^l + \epsilon[f(u_t^{l+1} - u_t^l) - f(u_t^l - u_t^{l-1})], \quad (8a)$$

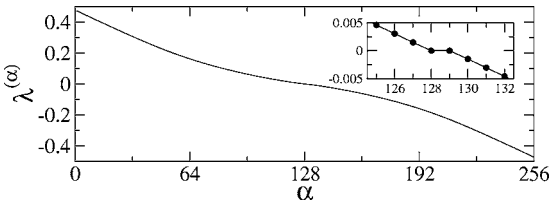

FIG. 1. Lyapunov spectrum for coupled standard maps Eq. (8) with $\epsilon = 0.6$. The enlargement in the inset shows that there is only one pair of zero-value Lyapunov exponents for this system. This implies that there is only one sort of HLMs in this simple system. The system size used is $L = 128$.

$$u_{t+1}^l = u_t^l + v_{t+1}^l, \quad (8b)$$

where $f(z)$ is a nonlinear map, t is the index for the discrete time, $l = \{1,2,\ldots,L\}$ is the index of the lattice site, and L is the system size. Unless it is explicitly stated otherwise, we set $f(z) = (1/2\pi)\sin(2\pi z)$ and use periodic boundary condition $\{u_t^0 = u_t^L,\ u_t^{L+1} = u_t^1\}$ for the numerical simulations shown below. And we set $\gamma_t^l = 0$ for the time being. Since the sympleticity condition $\Sigma_l du_t^l \times dv_t^l = \Sigma_l du_{t+1}^l \times dv_{t+1}^l$ is satisfied, this model corresponds to a Hamiltonian system.

Similar to many-particle systems such as Lennard-Jones fluids, the total-momentum-like quantity $P = \Sigma_l v_t^l$ is conserved during the iteration of the system dynamics. The system is also invariant with respect to an arbitrary translation of the whole system in the u direction.

For the one-dimensional lattice models studied in this paper, the position coordinate of the lth element is assigned simply as $r_l = la$ where a is the lattice constant. Then the LV fluctuation density is reduced to

$$\mathcal{U}^{(\alpha)}(x,t) = \sum_{l=1}^{L} \delta u_t^{(\alpha)l}\delta(x - la) \quad (9)$$

where $\{\delta u_t^{(\alpha)l}\}$ with $l = 1,2,\ldots,L$ is the coordinate-like part of the αth Lyapunov vector at discrete time t. The static and dynamic LV structure factors are formed analogously to Eqs. (3) and (7) as $S_u^{(\alpha\alpha)}(k) = \Sigma_{l=1}^{L} G_u^{(\alpha\alpha)}(la,0)e^{-jkla}$ and $S_u^{(\alpha\alpha)}(k,\omega) = \int \Sigma_{l=1}^{N} G_u^{(\alpha\alpha)}(la,t)e^{-jk\cdot l\cdot a}e^{j\omega t}dt$, respectively.

The Lyapunov spectrum of coupled standard maps with $\epsilon = 0.6$ is shown in Fig. 1. Here the spectrum is symmetric due to the symplectic structure of the system. From the enlargement shown in the inset of Fig. 1 one can see that there is only one pair of zero-value LEs for this model. They are related to the translational invariance of the system in the u direction and the existence of the conserved quantity P. It is believed that the zero-value LEs and the corresponding LVs are the organizing center for the part of the Lyapunov spectrum near zero and the corresponding HLMs. The existence of only one pair of zero-value LEs implies that only one sort of HLMs is possible here. Such a simple system with minimal complexity is very favorable for the study of the mechanisms for HLMs.

Two prototypical examples of the LVs are shown in Fig. 2. The LV associated with the largest positive LE ($\alpha = 1$) is highly localized while the one corresponding to the smalled

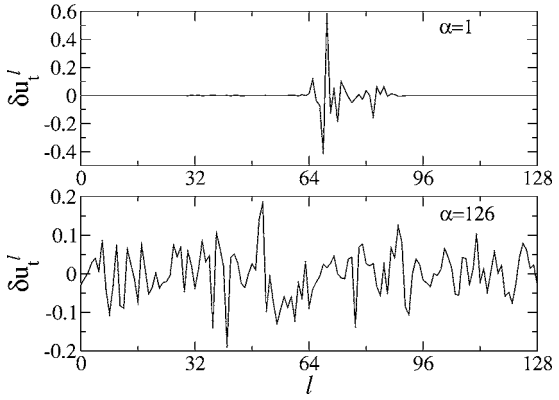

FIG. 2. Snapshots of the δu components of typical LVs for coupled standard maps Eq. (8) with parameters as in Fig. 1. The LV corresponding to the largest LE ($\alpha=1$) is highly localized while the one corresponding to a near zero LE ($\alpha=126$) is extended.

positive LE ($\alpha=126$) is extended. This is a general feature of LVs for an extended system and has been observed in various systems [36]. The contour plot of the static LV structure factor presented in Fig. 3 shows that for LVs with $\alpha \approx 128$, i.e., with $\lambda^{(\alpha)} \approx 0$, there is a sharp peak in the spectrum $S_u^{(\alpha\alpha)}(k)$. Furthermore, the position of the peak k_{max} approaches $2\pi/L$ as $\alpha \to 128$, i.e., as $\lambda^{(\alpha)}$ goes to 0^+ (see the lower panel of Fig. 3). Here $2\pi/L$ is the smallest nontrivial wave number allowed by the periodic boundary condition used. And the behavior of the LVs is qualitatively the same for all values of the coupling strength ϵ tested (see Fig. 4). These facts strongly suggest that HLMs exist in the system of coupled standard maps. Replacing the nonlinear function $f(z)$ by other one-dimensional maps like the logistic map or tent map yields qualitatively similar results. This finding enlarges greatly the regime where the HLMs are expected and implies that HLMs are generic for a large class of systems beyond the class of many-particle mechanical systems.

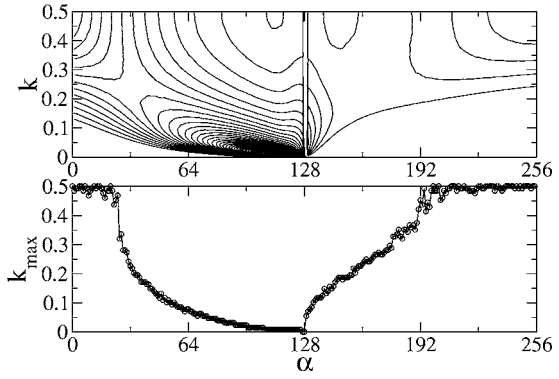

FIG. 3. Contour plot of the static LV structure factors (upper panel) and the dominant wave number k_{max} versus the index α of Lyapunov vectors (lower panel) for coupled standard maps Eq. (8) with the same parameter setting as in Fig. 1. The sharp dominant peaks in the static LV structure factors with $k_{max} \to 0$ as $\alpha \to 128$ indicate the existence of HLMs in this system. The unit 2π is used for the wave number k in all concerned figures throughout this paper.

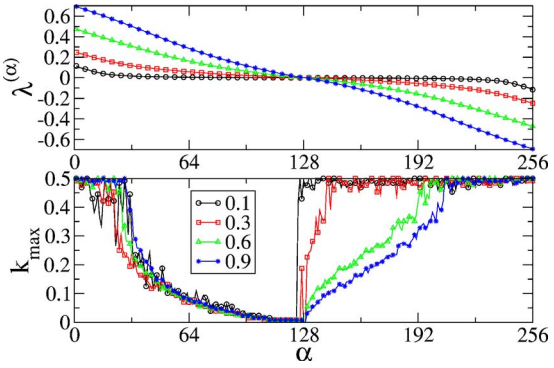

FIG. 4. (Color online) Lyapunov spectra (upper panel) and the peak wave number k_{max} (lower panel) versus the index α for coupled standard maps Eq. (8) with coupling strength $\epsilon=0.1$, 0.3, 0.6, and 0.9. Changing the value of ϵ does not change the fact that $k_{max} \to 0$ as $\alpha \to 128$, i.e., the existence of HLMs does not change. The system size used is $L=128$.

IV. IS A HAMILTONIAN STRUCTURE NEEDED FOR HLMS?

Now we turn to our second model which is a lattice of circle maps with force-like couplings,

$$u_{t+1}^l = (1-\gamma_t^l)u_t^l + \epsilon[f(u_t^{l+1}-u_t^l) - f(u_t^l - u_t^{l-1})], \quad (10)$$

where again $f(z)=(1/2\pi)\sin(2\pi z)$ and $\gamma_t^l=0$ is set for the moment. Now the quantity $Q=\Sigma_l u_t^l$ is conserved during the time evolution of the system dynamics. And the system is again invariant under an arbitrary translation in the u direction. An essential difference from the model of coupled standard maps in Eq. (8) is that the current system is dissipative because phase space volume is contracting with time going on.

Results of numerical simulations for this model with $\epsilon=1.3$ are displayed in Fig. 5. The Lyapunov spectrum is no longer symmetric as for the case of coupled standard maps due to the dissipative nature of the system. The behavior of the static LV structure factors are quite similar to the case of

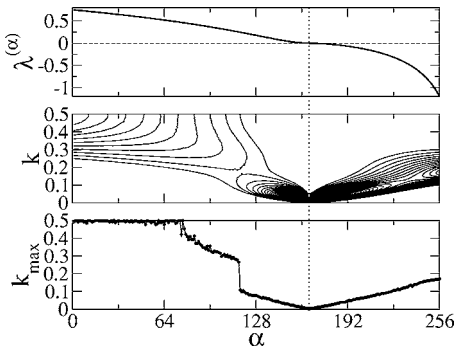

FIG. 5. Lyapunov spectrum (top panel), the contour plot of the static LV structure factors $S_u^{(\alpha\alpha)}(k)$ (middle panel), and the peak wave-number k_{max} (bottom panel) for coupled circle maps with force-like coupling given in Eq. (10) with $\epsilon=1.3$. The sharp dominant peaks in the spectra $S_u^{(\alpha\alpha)}(k)$ with $k_{max} \to 0$ as $\alpha \to 164$ imply the existence of HLMs in this system. The system size used is $L=256$.

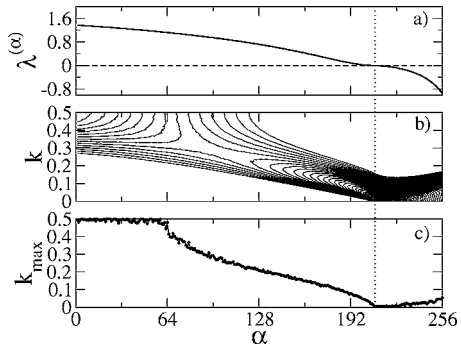

FIG. 6. (a) The Lyapunov spectrum, (b) contour plot of $S_u^{(\alpha\alpha)} \times(k)$, and (c) k_{max} versus the index α of the LVs for the Bohr model Eq. (11) with $\epsilon=1.0$. The system size used is $L=256$.

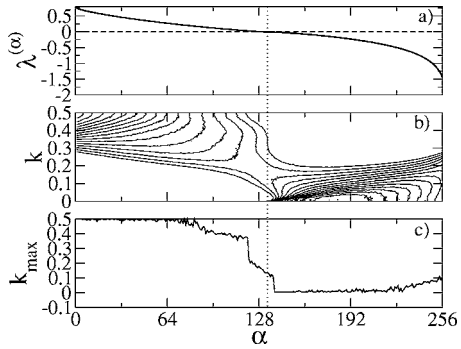

FIG. 7. Similar to Fig. 6 but with $\epsilon=0.58$. In the bottom panel the wave number k_{max} for the dominant peak of the spectrum of each LV is plotted versus α. It can be easily seen that k_{max} attains a finite value as $\lambda^{(\alpha)} \to 0$. This shows that there exist no HLMs in this system.

coupled standard maps. The spectra $S_u^{(\alpha\alpha)}$ for LVs with $\alpha \approx 164$ ($\lambda^{(\alpha)} \approx 0$) are significantly dominated by certain long wavelength components and the wave number of the dominant peak $k_{max} \to 2\pi/L$ as $\lambda^{(\alpha)} \to 0$. Tuning the coupling strength ϵ leads to no qualitative changes in the behavior of LVs. These simulations demonstrate that HLMs are also possible for dissipative systems with a conserved quantity and translational invariance. Therefore, the Hamiltonian structure is not a necessary condition for the existence of HLMs.

One may notice that for the case studied here the static LV structure factors and the peak wave number k_{max} behave qualitatively similar on both side of $\lambda=0$. This implies that for this system HLMs exist not only on the positive side but also on the negative LE side.

V. COUPLED MAP LATTICE WITH CONSERVED QUANTITY BUT LACK OF TRANSLATIONAL INVARIANCE

Let us further relax the constraints for the system considered and see how the HLMs are changed. The model below belongs to the class used by Bohr *et al.* [22,37] in the study of Lyapunov spectrum condensation. It reads

$$x_{t+1}^l = x_t^l + \epsilon[f(x_t^{l+1}) + f(x_t^{l-1}) - 2f(x_t^l)]. \tag{11}$$

We set $f(z)=(1/2\pi)\sin(2\pi z)$ and use again periodic boundary conditions $\{x_t^0=x_t^L,\ x_t^{L+1}=x_t^1\}$ for the following numerical simulations. The system is designed to conserve the quantity $Q=\Sigma_l x_t^l$ during iterations. Here the coupling among neighbor sites is diffusive, which is commonly used in the construction of CMLs [19]. The replacement of the force-like coupling in Eq. (10) by a diffusive one breaks the system's translational invariance in u space. We will see how this change influences the behavior of LVs.

Figure 6 shows the results of simulations for the Bohr model with $\epsilon=1.0$. The contour plot of $S_u^{(\alpha\alpha)}(k)$ demonstrates clearly that for each LV with $\lambda^{(\alpha)} \approx 0$ there exists a peak in its spectrum. To make the situation clear, the wave number k_{max} for the dominant peak is plotted, versus the index α of LVs. One can see that k_{max} decreases gradually as α goes to 209 (i.e., as $\lambda^{(\alpha)}$ goes to zero). If one stops to do further numerical experiments, one may think that HLMs exist in this system as in the case of circle maps with force-like coupling. However, with decreasing coupling strength, for instance for the case with $\epsilon=0.58$, one can see clearly that k_{max} attains a finite value $k_0 \gg 2\pi/L$ as $\lambda^{(\alpha)}$ decreases to zero (cf. Fig. 7). This means that the corresponding LVs are not long wavelength modes on a hydrodynamical time scale. A careful study of the case with $\epsilon=1.0$ shows that there k_{max} also approaches a finite value $k_0 \approx 8\pi/L$ as $\lambda^{(\alpha)} \to 0$, which is comparable to but different from the minimal value $2\pi/L$ allowed by the periodic boundary conditions.

One may notice that the diffusively coupled model studied here is simply related to the model with force-like coupling studied in the last section [Eq. (10)] via a variable transformation $x_t^l = u_t^{l+1} - u_t^l$. This connection implies the possibility that there exists some relation between the Lyapunov spectra and Lyapunov vectors of the two models. Comparisons of the Lyapunov spectra, static LV structure factors, and peak wave number k_{max} of the two models are shown in Fig. 8. To obtain an one-to-one mapping between the two models with different coupling forms, the fixed boundary conditions $\{x_t^0=0,\ x_t^{L+1}=0\}$ are applied to the Bohr model while the boundary conditions $\{u_t^0=0,\ u_t^{L+1}=u_t^L\}$ are imposed to the coupled circle maps with force-like coupling. From the plot one can see that the Lyapunov spectra of the two models are nearly identical. Actually, it is known that the Lyapunov spectrum is invariant under linear transformations. The static LV structure factors, however, are obviously different. The values of k_{max} are also different especially on the side of positive LEs.

Considering the linear transformation $x_t^l = u_t^{l+1} - u_t^l$ between the variables of the two models, it is plausible to assume that in the regime $\lambda \simeq 0$ the Lyapunov vectors $\Gamma_u^{(\alpha)} \equiv \{\delta u_t^{(\alpha)l}\}$ for the model in Eq. (10) and $\Gamma_x^{(\alpha)} \equiv \{\delta x_t^{(\alpha)l}\}$ for the model in Eq. (11) are related via

$$\delta x_t^{(\alpha)l} = \delta u_t^{(\alpha)l+1} - \delta u_t^{(\alpha)l}. \tag{12}$$

The LV fluctuation densities of the two systems are defined as

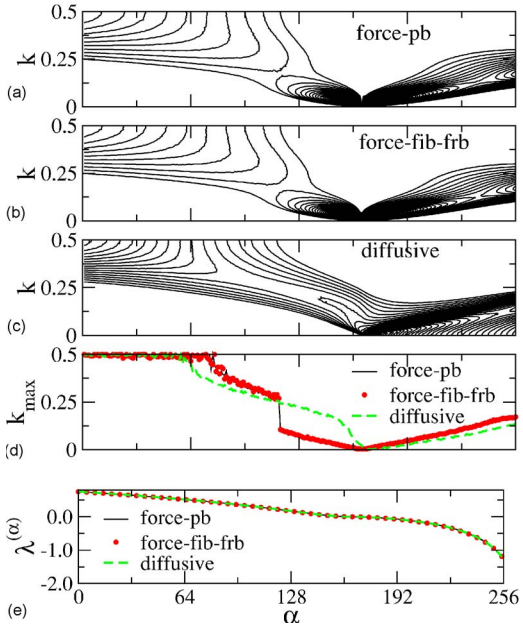

FIG. 8. (Color online) (a)–(c) Contour plot of $S_u^{(\alpha\alpha)}(k)$ for the coupled circle map with boundary condition $\{u_t^0=u_t^L,\ u_t^{L+1}=u_t^1\}$ (*force-pb*), $\{u_t^0=0,\ u_t^{L+1}=u_t^L\}$ (*force-fib-pb*), respectively, and for the Bohr model Eq. (11) with $\{x_t^0=0,\ x_t^{L+1}=0\}$ (*diffusive*). The coupling strength used is $\epsilon=1.3$. Panel (d) shows the peak wave number k_{max} for the three cases. An obvious difference between the case of *force-fib-pb* and *diffusive* can be seen. Panel (e) shows the Lyapunov spectra for the three cases. They are nearly identical. The system size used is $L=256$.

$$\mathcal{U}^{(\alpha)}(r,t)=\sum_{l=1}^{L}\delta u_t^{(\alpha)l}\delta(r-la), \tag{13a}$$

$$\mathcal{X}^{(\alpha)}(r,t)=\sum_{l=1}^{L}\delta x_t^{(\alpha)l}\delta(r-la), \tag{13b}$$

respectively. Adopting the new variables $\mathcal{U}_k^{(\alpha)}(t)=\int\mathcal{U}^{(\alpha)}\times(r,t)\exp(-jkr)dr$ and $\mathcal{X}_k^{(\alpha)}(t)=\int\mathcal{X}^{(\alpha)}(r,t)\exp(-jkr)dr$, the LV fluctuation densities can be written as

$$\mathcal{U}^{(\alpha)}(r,t)=\sum_k\mathcal{U}_k^{(\alpha)}(t)\exp(jkr), \tag{14a}$$

$$\mathcal{X}^{(\alpha)}(r,t)=\sum_k\mathcal{X}_k^{(\alpha)}(t)\exp(jkr). \tag{14b}$$

Then the static LV structure factors of the two models take the form

$$S_u^{(\alpha\alpha)}(k)=\langle\|\mathcal{U}_k^{(\alpha)}(t)\|^2\rangle, \tag{15a}$$

$$S_x^{(\alpha\alpha)}(k)=\langle\|\mathcal{X}_k^{(\alpha)}(t)\|^2\rangle. \tag{15b}$$

The linear relation in Eq. (12) implies in the long wavelength limit (for $a=1$)

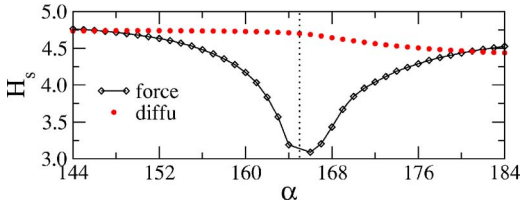

FIG. 9. (Color online) Spectral entropy [38] $H_S\equiv-\Sigma_{k_i}S(k_i)\ln S(k_i)$ vs. α of force-like coupled and diffusively coupled circle maps with $\epsilon=1.3$. The smaller value of H_S for the force-like coupled model means the HLMs are more significant there than in the case with diffusive coupling.

$$\mathcal{X}_k^{(\alpha)}(t)=jk\mathcal{U}_k^{(\alpha)}(t). \tag{16}$$

Inserting Eq. (16) in Eq. (15) leads to a relation between the static LV structure factors of the two models

$$S_x^{(\alpha\alpha)}(k)=k^2S_u^{(\alpha\alpha)}(k). \tag{17}$$

Despite the use of mathematically nonrigorous assumptions, the obtained relation in Eq. (17) can explain that the dominant peaks in the static LV structures of the force-like coupled maps are much more pronounced than those in the corresponding case with diffusive coupling. As can be seen in Fig. 9, the spectral entropy $H_S\equiv-\Sigma_{k_i}S(k_i)\ln S(k_i)$ [38] for the force-like coupling is much smaller than those of the diffusively coupled maps, which means that the coherent wave structures are much weaker in the diffusively coupled maps than in the model with force-like coupling.

Equation (17) provides also a rough criterion for the possibility of observing HLMs in diffusively coupled systems if they are detected in the corresponding system with force-like coupling. To be concrete, the decreasing of $S_u^{(\alpha\alpha)}(k)$ vs. k should be faster than k^{-2} in the regime $k\geqslant k_{max}$, otherwise the dominant peak in $S_x^{(\alpha\alpha)}(k)$ will no longer be at the same position as in $S_u^{(\alpha\alpha)}(k)$ and consequently it is possible that k_{max} of $S_x^{(\alpha\alpha)}(k)$ attains a finite nonzero value as λ goes to zero. The criterion works quite well for many cases checked even though the relation in Eq. (17) itself is found to be correct only qualitatively (see Fig. 10). As an example, the static LV structure factor for LV with $\alpha=163$ of the same system as used in Fig. 8 is plotted with k in Fig. 11. Here $S_u^{(\alpha\alpha)}(k)\sim k^{-1.4}$ for $k\simeq 2\pi/L$. According to the criterion, the values of k_{max} extracted from the two models are different (see Fig. 8) and there are no HLMs in the model with diffusive coupling. The case shown in Fig. 12 is for the coupled skewed tent map [40]. Now $S_u^{(\alpha\alpha)}(k)\sim k^{-2.2}$ in the regime $k\geqslant 0$ for LV with $\alpha=179$. This ensures that the values of k_{max} obtained are identical for the two models with different types of couplings [see panel (a) of Fig. 12]. It also means that long wavelength structures can also be observed in the diffusively coupled system in this case. For the case with $f(z)=2z$ (mod 1), where the assumption in Eq. (12) is fulfilled, therefore the result shown in Eq. (17) is valid exactly, the tangent space dynamics is identical to the corresponding case with force-like coupling. We refer to Sec. IX for the analytical treatment of this case.

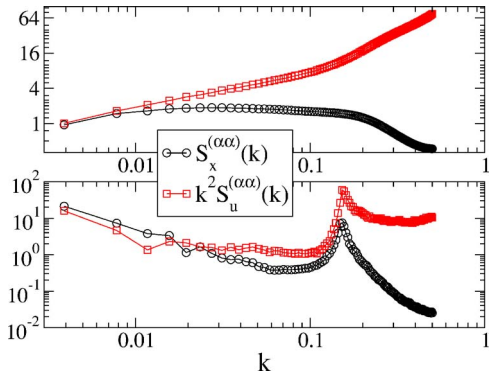

FIG. 10. (Color online) Comparison of the two quantities $S_x^{(\alpha\alpha)} \times(k)$ and $k^2 S_u^{(\alpha\alpha)}(k)$ for coupled circle maps (upper panel) and coupled skewed tent maps (lower panel). The agreement of the two quantities in the regime $k \simeq 2\pi/L$ implies that the assumption in Eq. (12) used for deducing Eq. (17) is plausible.

VI. COUPLED MAP LATTICE WITH TRANSLATIONAL INVARIANCE BUT LACK OF CONSERVED QUANTITY

For Hamiltonian or Lagrangian systems there is a one-to-one correspondence between conserved quantities and symmetries according to the celebrated Noether's theorem [41], e.g., momentum conservation is related to space translation invariance. In general there is no such correspondence for general dynamical system. As we saw already in the Bohr model studied in the last section, a system possessing a conserved quantity may lack translational invariance. In this section we will investigate the counterpart where translational invariance is kept while no conserved quantity exists.

The system is of the form

$$v_{t+1}^l = v_t^l + \epsilon[f(u_t^{l+1} - u_t^l) - g(u_t^l - u_t^{l-1})], \tag{18a}$$

$$u_{t+1}^l = u_t^l + v_{t+1}^l, \tag{18b}$$

where the coupling to the left neighbor is different from the one to the right neighbor. As an example, we show in Fig. 13 the results of simulations for the case with $f(z) = (1/2\pi)\sin(2\pi z)$ and $g(z) = (1/2\pi)\cos(2\pi z)$. The Lyapunov spectrum is still symmetric although the Hamiltonian structure is destroyed. However, no significant peak can be detected from the static LV structure factors. The numerically extracted k_{max} has a finite value at $\lambda \approx 0$. This implies that HLMs do not exist in this model system, i.e., the translational invariance alone cannot guarantee their existence.

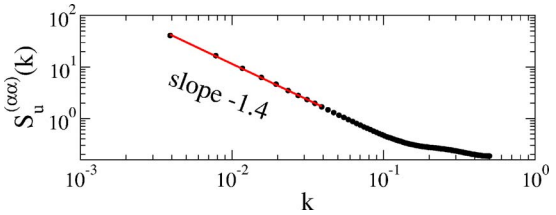

FIG. 11. (Color online) Static LV structure factor $S_u^{(\alpha\alpha)}(k)$ for LV with $\alpha=163$ of force-like coupled circle maps [Eq. (10)]. Here $k_{max}=2\pi/L$ and the power law fitting gives $S_u^{(\alpha\alpha)}(k) \sim k^{-1.4}$ in the regime $k \geqslant k_{max}$. According to Eq. (17), the values of k_{max} extracted from the two models with different couplings should be different (see Fig. 8) and there exist no HLMs in the model with diffusive couplings. The zero-value Lyapunov exponent is at $\alpha=164$.

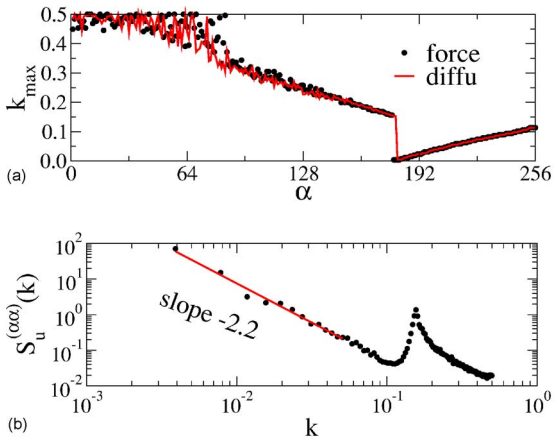

FIG. 12. (Color online) (a) Peak wave number k_{max} vs. α for the force-like and diffusively coupled skewed tent maps [40] with $r=5$. (b) Static structure factor $S_u^{(\alpha\alpha)}(k)$ for the LV with $\alpha=179$. Here $k_{max}=2\pi/L$ and the power law fitting gives that $S_u^{(\alpha\alpha)}(k) \sim k^{-2.2}$ in the regime $k \geqslant k_{max}$. According to the criterion [Eq. (17)], the values of k_{max} extracted from the two models with different couplings should be identical (see the numerical results shown in panel a). The zero-value Lyapunov exponent is at $\alpha=178$. For this case, the HLMs only exist for the negative branch of Lyapunov spectrum ($\alpha>178$). The reason for this and the jump in k_{max} is not important for the current discussion.

We also investigated the dissipative system

$$u_{t+1}^l = u_t^l + \epsilon[f(u_t^{l+1} - u_t^l) - g(u_t^l - u_t^{l-1})]. \tag{19}$$

Numerical simulations for the case with $f(z) = (1/2\pi)\sin(2\pi z)$ and $g(z) = (1/2\pi)\cos(2\pi z)$ show that HLMs do not exist in this model system. This demonstrates again that the translational invariance alone cannot guarantee the existence of HLMs.

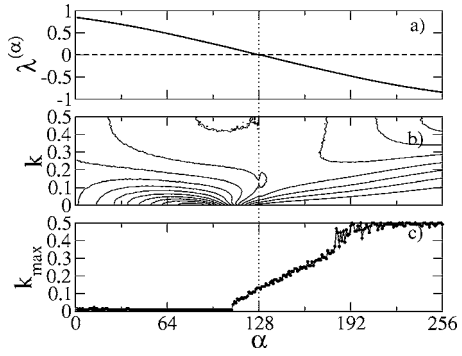

FIG. 13. (a) The Lyapunov spectrum, (b) contour plot of $S_u^{(\alpha\alpha)} \times(k)$, and (c) k_{max} versus α for the model Eq. (18) with $\epsilon=1.0$. There is no sharp peak in the spectra $S_u^{(\alpha\alpha)}(k)$ and the k_{max} extracted attains a finite value $k_0 \geqslant 2\pi/L$ as $\lambda^{(\alpha)} \to 0$, which implies that there are no HLMs in this model. The system size used here is $L=128$.

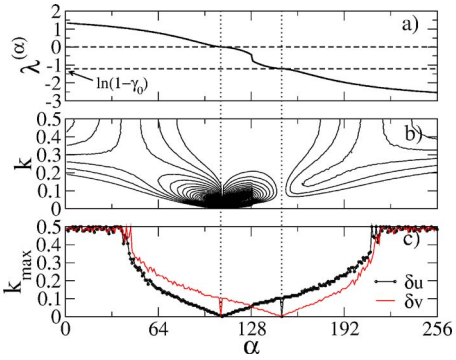

FIG. 14. (Color online) (a) The Lyapunov spectrum, (b) contour plot of $S_u^{(\alpha\alpha)}(k)$, and (c) k_{max} versus α for coupled standard maps under damping with $\epsilon=2.3$, $\gamma_0=0.7$, and $L=128$. Although the Lyapunov spectrum is no longer symmetric with respect to $\lambda^{(\alpha)}=0$, there is still $k_{max}\to 2\pi/L$ as $\lambda^{(\alpha)}\to 0$, i.e., HLMs survive damping in this system. Note that, in panel (c), the two curves for the coordinate and momentum parts of the Lyapunov vectors are mutual mirror images due to the μ-symplectic structure of the system treated here [39].

VII. CAN DAMPING DESTROY THE HLMS?

In investigations of hard-ball systems, Hirschl and Posch also found the HLMs in the nonequilibrium case of color conduction, where the system is globally thermostatted and damped [7]. Here we introduce a damping term into our models to see its impact. For the coupled circle maps in Eq. (10), we let $\gamma_t'=\gamma_0\in[0,1)$, which leads to the shrinking of the quantity Q as $Q_{t+1}=(1-\gamma_0)Q_t$. For the case of coupled standard maps in Eq. (8), $\gamma_t'=\gamma_0\in[0,1)$ causes the shrinking of $P=\Sigma_l v_t^l$ correspondingly.

Results of simulations for the two models with damping are presented in Figs. 14 and 15 respectively. For coupled damped standard maps the Lyapunov spectrum satisfies the relation $\lambda^{(\alpha)}+\lambda^{(2L+1-\alpha)}=\ln(1-\gamma_0)$ instead of $\lambda^{(\alpha)}=-\lambda^{(2L+1-\alpha)}$. The spectrum is still symmetric but the symmetry center is no longer at $\lambda^{(\alpha)}=0$ but at $\lambda^{(\alpha)}=\frac{1}{2}\ln(1-\gamma_0)$. The symmetry of the Lyapunov spectrum has its origin in the well-known μ-symplectic structure of Hamiltonian systems with damping or thermostats [39]. The damping also leads to a gap in the Lyapunov spectrum at its symmetry center. Comparing with Fig. 3 one can see that the static LV structure factor changes strongly under the influence of the damping. For LVs with $\lambda^{(\alpha)}\approx 0$, however, there is still $k_{max}\to 2\pi/L$ with $\lambda^{(\alpha)}\to 0$ as in the case without damping. Hence the introduction of damping in a system of coupled Hamiltonian maps does not destroy the HLMs. Actually, one might have expected such a result, since the model of coupled circle maps Eq. (10) is just the over-damped case of coupled standard maps Eq. (8) with $\gamma_t'=1$. In panel (c) of Fig. 14, the dependence of k_{max} on α is shown for both the coordinate and momentum parts of Lyapunov vectors. If we denote the two parts of a Lyapunov vector as $\Gamma_u^{(\alpha)}$ and $\Gamma_v^{(\alpha)}$, respectively, the μ-symplectic structure of the system treated here leads to the conjugate relation $\Gamma_v^{(\alpha)}=-\Gamma_u^{(2L+1-\alpha)}$ [39]. Note that, due to this relation, the two curves in panel (c) of Fig. 14 are mutual mirror images.

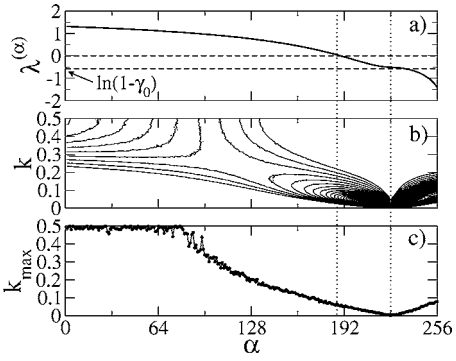

FIG. 15. (a) The Lyapunov spectrum, (b) contour plot of $S_u^{(\alpha\alpha)}\times(k)$, and (c) k_{max} versus α for coupled circle maps under damping with $\epsilon=2.3$, $\gamma_0=0.4$, and $L=256$. In contrast to Fig. 14 HLMs are not observed in this system since k_{max} attains a finite $k_0\gg 2\pi/L$ as $\lambda^{(\alpha)}\to 0$.

In contrast to this, for the case of damped coupled circle maps the point of $k_{max}\approx 0$ moves to $\lambda=\ln(1-\gamma_0)$ (see Fig. 15). The LVs with $\lambda\approx 0$ are no longer of wavelength comparable to the system size, i.e., the damping wipes off the HLMs in the system of coupled circle maps.

For the system of coupled standard maps, we have simulated also the case with spatially inhomogeneous damping $\gamma_t'=\gamma'$. Now, there is no general relation between P_{t+1} and P_t. The behavior of the LVs is, however, similar to the case with homogeneous damping $\gamma_t'=\gamma_0$.

Note that coupled map lattices with damping bear some similarity to thermostated systems. Thermostats are powerful numerical devices used to mimic the situation when the system under investigation is in contact with a heat bath. For Gaussian isokinetic and isoenergetic deterministic thermostats, a fictitious damping term is introduced into the original Hamiltonian dynamics [39]. Since the energy flow between the heat bath and the treated system is bidirectional, the damping coefficient can be either negative or positive depending on the instantaneous states of the system. In view of this, we simulated coupled standard maps with time-dependent random damping, i.e., $\gamma_t'=\gamma_t$ are taken from time-dependent random numbers with an uniform distribution in the interval $[-\gamma_1,\gamma_1]$. Numerical simulations for several cases with different coupling strengths ϵ and constants γ_1 yield similar results as presented in Fig. 14. Therefore, we expect that a similar scenario as shown above should be found in nonequilibrium many-particle systems with thermostats.

Note that $\gamma_t'\neq 0$ breaks translational invariance for the case of coupled circle maps but not for coupled standard maps.

VIII. INFLUENCE OF AN ON-SITE POTENTIAL

From the simulations shown so far, one may doubt whether the conservation laws are really necessary for the existence of HLMs. Here we continue the experiment in this direction and introduce one more term in our models to mimic an on-site potential, which can destroy the conservation laws. For the model of coupled circle maps we added a

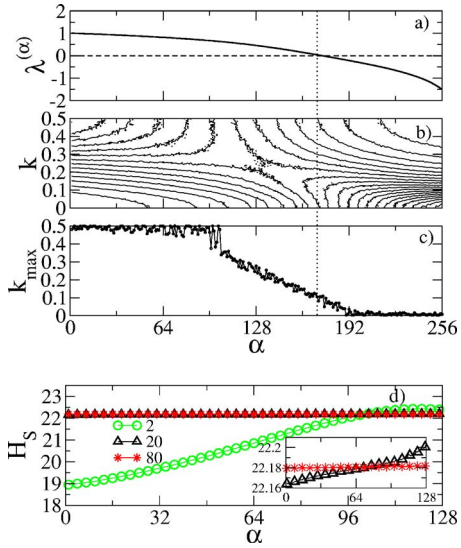

FIG. 16. (Color online) (a)–(c) Results of simulations for coupled circle maps with on-site potential with $\epsilon=1.3$, $\kappa=2.0$, and $L=256$. (d) Spectral entropy H_S for the coupled standard maps with $\epsilon=0.3$, $L=128$, and $\kappa=2$, 20, and 80, respectively. These results show that the on-site potential strongly influences the behavior of LVs and destroys the hydrodynamic Lyapunov modes.

term $\kappa f(u_t^l)$ to the right-hand side of Eq. (11). For the case of coupled standard maps the term $\kappa f(u_t^l)$ is added to the right-hand side of Eq. (8a). Results of the simulations are shown in Fig. 16. For both cases, the static LV structure factors $S_u^{(\alpha\alpha)}(k)$ become quite homogeneous. No sharp peaks can be distinguished even for those LVs with $\lambda \approx 0$. If one nevertheless extracts a k_{max} from the spectra as done before, one finds for the model of coupled circle maps that k_{max} attains a nonzero value at $\lambda^{(\alpha)}=0$. To further characterize the spectra, we calculated the spectral entropy as for Fig. 9. For the model of coupled standard map, three cases with $\kappa=2$, 20, and 80 are presented in Fig. 16. With increasing κ, the variation of H_S with α becomes weaker and weaker. Actually, even for the case with $\kappa=2$, the smallest value of H_S attained at $\alpha=0$ is already not far from the value $H_0=22.18$ for a homogeneous spectrum $S(k_i)=0.5$ with $k_i=2\pi/L, 4\pi/L, \ldots, \pi$. This simulation shows that the on-site potential strongly influences the behavior of LVs and destroys the hydrodynamic Lyapunov modes.

IX. UNIVERSALITY CLASSES OF THE λ-*k* DISPERSION RELATIONS

One important characterization of the HLMs is their dispersion relation defined as $\lambda \sim k_{max}^{\beta}$, where k_{max} is the dominating wave number of a LV and $\lambda^{(\alpha)}$ is the value of the LE associated with this LV. In comparison with the relation $\lambda^{(\alpha)}$ vs. α used to study the universal shape of Lyapunov spectra [42], the dispersion relation defined here is more suitable for the characterization of Lyapunov vectors, since the quantity k_{max} can provide important information about their spatial structures. Such a dispersion relation has been used to investigate HLMs in many-particle systems [8,15].

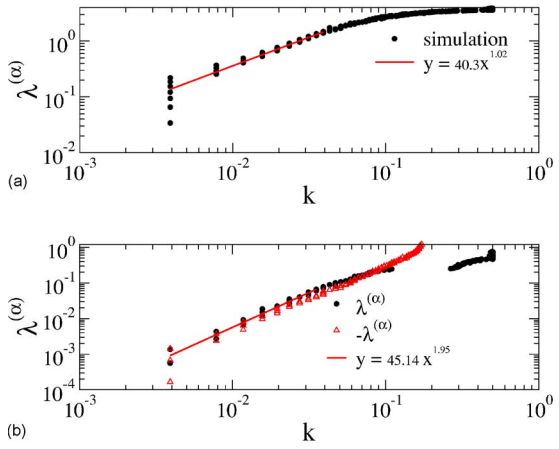

FIG. 17. (Color online) Dispersion relation $\lambda^{(\alpha)}$ vs. k for (a) coupled standard maps Eq. (8) and (b) coupled circle maps Eq. (10). Fitting of the data to a power law function $\lambda^{(\alpha)} \sim k^{\beta}$ yields $\beta \approx 1.0$ for the coupled standard maps and $\beta \approx 2.0$ for the coupled circle maps.

The dispersion relation for coupled standard maps is presented in the upper panel of Fig. 17. Numerical fitting of the small k and λ part to a power-law function gives $\lambda \sim k^{\beta}$ with $\beta=1.02$. A similar fitting for the case of circle maps with force-like coupling yields $\beta=1.95$ (see the lower panel of Fig. 17). These values were checked by simulations with different coupling strength ϵ and system size L. It appears that the two models belong to two different universality classes with either $\beta=1.0$ or $\beta=2.0$. Simulations for systems with different choices of the nonlinear function $f(z)$, e.g., for a parabolic or piecewise linear $f(z)$, support our conjecture of two universality classes.

Although we cannot provide a general analytical proof of the existence of these two universality classes, there are special cases where the dispersion relations can be obtained analytically. If the nonlinear function $f(z)=(1/2\pi)\sin(2\pi z)$ in Eq. (10) is replaced by the Bernoulli shift map $f(z)=2z \pmod 1$, the dynamics of the linearized perturbation in the tangent space is governed by $\delta\vec{U}_{t+1}=(I_L+2\epsilon D_L)\cdot\delta\vec{U}_t$, where $\delta\vec{U}_t$ is the vector formed by the perturbations of individual elements at the time step t and we use I_L and D_L to denote the $(L \times L)$-unit matrix and the discrete Laplacian, respectively. One can easily obtain that eigenvalues of the matrix $I_L+2\epsilon D_L$ are of the form $\mu(k)=1-4\epsilon(1-\cos k)$ and the associated eigenvectors are $\vec{e}^{(\alpha)} \equiv \{\delta u_l^{(\alpha)}\}$ with $\delta u_l^{(\alpha)} = a_1 \cos(k \cdot la) + a_2 \sin(k \cdot la)$ where l is the index of lattice site, a_1 and a_2 are two constants [43], and $k=2\pi(\alpha-1)/L$ for $\alpha=\{1,2,3,\ldots,L\}$. Since the matrix $M_1=I_L+2\epsilon D_L$ is time independent and $M_1^T=M_1$, it can be easily shown that the Lyapunov exponents are simply $\lambda \equiv \ln|\mu(k)|$ and the Lyapunov vectors are just the eigenvectors of M_1. As $k \to 0$, the Lyapunov exponents vary quadratically,

$$\lambda(k) = \ln|1 - 4\epsilon(1 - \cos k)| \simeq 2|\epsilon|k^2, \tag{20}$$

i.e., the HLMs in force-like coupled Bernoulli shift maps are characterized by the dispersion relation $\lambda \sim k^2$.

The linearized equations for the model of coupled Hamiltonian maps Eq. (8) with $f(z)=2z \pmod 1$ are of the form

$$\delta\vec{\Gamma}_{t+1} = \begin{pmatrix} I_L + 2\epsilon D_L & I_L \\ 2\epsilon D_L & I_L \end{pmatrix} \cdot \delta\vec{\Gamma}_t,$$

where $\delta\vec{\Gamma}_t \equiv \{\delta u_t^1, \delta u_t^2, \ldots, \delta u_t^L; \delta v_t^1, \delta v_t^2, \ldots, \delta v_t^L\}$ is the offset vector in the tangent space. The eigenvectors of the fundamental matrix

$$M_2 \equiv \begin{pmatrix} I_L + 2\epsilon D_L & I_L \\ 2\epsilon D_L & I_L \end{pmatrix}$$

can be easily constructed as $\{\vec{e}^{(\alpha)}; c(k)\vec{e}^{(\alpha)}\}$ using the eigenvectors $\vec{e}^{(\alpha)}$ of the matrix D_L. The associated eigenvalues are

$$\mu_{1,2}(k) = \frac{\eta + 2 \pm \sqrt{\eta^2 + 4\eta}}{2} \tag{21}$$

where $\eta(k) = -4\epsilon(1-\cos k)$ and the corresponding $c(k)$ can be easily calculated as

$$c_{1,2}(k) = \mu_{1,2} - 1 - \eta. \tag{22}$$

In Eq. (21), the subscripts 1 and 2 are corresponding to the positive and negative signs on the r.h.s., respectively.

We now have to provide the relation of Lyapunov exponents and Lyapunov vectors to the eigenvalues and eigenvectors of the matrix M_2. Since the matrix M_2 is time independent, the eigenvalues of the matrix product M_2^N, which is the so-called stability matrix [31], are simply $\mu(k)^N$ and the eigenvectors are identical to those of M_2. An important result of Ref. [31] is that generically $\lambda \equiv \ln|\mu(k)|$ where λ are the Lyapunov exponents. According to Ref. [32], the Lyapunov vectors $\mathbf{f}^{(\alpha)}$ are the eigenvectors of the matrix $\bar{\bar{\Xi}} \equiv \lim_{N\to+\infty}[(M_2^{-N})^T \cdot M_2^{-N}]^{1/2N}$, which is the Oseledec matrix for the time-inverse dynamics of the original system. As demonstrated in Ref. [31], upon performing a Gram-Schmidt orthogonalization procedure on the set of eigenvectors $\{\mathbf{e}^{(\alpha)}\} = \{\mathbf{e}^{(1)}, \mathbf{e}^{(2)}, \ldots, \mathbf{e}^{(2\mathbf{L})}\}$ of the matrix M_2^{-N}, which is the stability matrix of the time-inverse dynamics of the original system, one obtains an orthonormal set, which approaches asymptotically for long times the eigenvectors $\mathbf{f}^{(\alpha)}$ of the matrix $\bar{\bar{\Xi}}$. Notice that the orthogonalization procedure starts from the last vector $\mathbf{e}^{(2L)}$. It is easy to obtain the αth eigenvector of the matrix M_2^{-N} as $\mathbf{e}^{(\alpha)} = \{\vec{e}^{(2L+1-\alpha)}; c_\nu^\nu(k)\vec{e}^{(2L+1-\alpha)}\}$ and the associated eigenvalue $\mu_\nu(k)^{-N}$ where $\nu=1$ for $L+1 \leqslant \alpha \leqslant 2L$ and $\nu=2$ for $1 \leqslant \alpha \leqslant L$. Upon performing a Gram-Schmidt orthogonalization procedure on $\{\mathbf{e}^{(\alpha)}\}$ one gets the Lyapunov vectors $\mathbf{f}^{(\alpha)} = \{\vec{e}^{(\alpha)}; c_1(k)\vec{e}^{(\alpha)}\}$ for $1 \leqslant \alpha \leqslant L$ and $\mathbf{f}^{(\alpha)} = \{-c_1(k)\vec{e}^{(\alpha)}; \vec{e}^{(\alpha)}\}$ for $L+1 \leqslant \alpha \leqslant 2L$. For simplicity, we ignored the normalization factors for these vectors in the above discussion.

As $k \to 0$, for the case with $\epsilon < 0$ [44], the Lyapunov exponents are approximated by

$$\lambda(k) \simeq \sqrt{2|\epsilon|}k. \tag{23}$$

Therefore the dispersion relation for coupled Hamiltonian maps is $\lambda \sim k^\beta$ with $\beta = 1.0$. The results of numerical simulations for the model system Eqs. (8) and (10) with $f(z)=2z \pmod 1$ are presented in Figs. 18 and 19, respectively. As expected they are in agreement with our above analytical calculations.

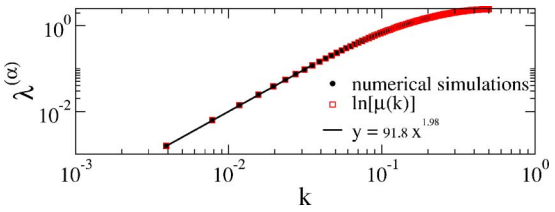

FIG. 18. (Color online) The dispersion relation $\lambda^{(\alpha)}$ vs. k for the model Eq. (10) with $f(z)=2z \pmod 1$ and $\epsilon=-1.3$. The analytical expression $\lambda = \ln[1-4\epsilon(1-\cos k)]$ has a perfect agreement with the numerical simulations.

For many-particle systems with hard-core interaction, Posch *et al.* proposed a linear dependence of λ on k. The simulation results for Lennard-Jones fluids were fitted with a power law $\lambda \sim k^{1.2\pm0.1}$, which is not far from a linear dispersion relation. Both simulations are for systems with particle numbers from hundreds to thousand, which is far from the thermodynamic limit. We therefore attribute the above deviations from the linear dispersion to finite size effects and conjecture that both systems belong to the universality class with $\lambda \sim k$.

Now we investigate in more detail how damping influences the dispersion relation. Let us start from the simple cases with $f(z)=2z \pmod 1$ and homogeneous damping $\gamma_t' = \gamma_0$ and do similar calculations as above. For the model of Eq. (10), the linearized equation now takes the form $\delta\vec{U}_{t+1} = [(1-\gamma_0)I_L + 2\epsilon D_L] \cdot \delta\vec{U}_t$. The Lyapunov exponents become $\lambda(k) = \ln|1-\gamma_0-4\epsilon(1-\cos k)|$. As $k \to 0$, they approach $\lambda \simeq \ln(1-\gamma_0)$. The nonzero values of the Lyapunov exponents for $k \to 0$ implies that HLMs do not exist for this case. This is in agreement with the numerical results obtained above (see Fig. 15).

For the model of Eq. (8) with $\gamma_t' = \gamma_0 \neq 0$, the linearized equations become

$$\delta\vec{\Gamma}_{t+1} = \begin{pmatrix} I_L + 2\epsilon D_L & (1-\gamma_0)I_L \\ 2\epsilon D_L & (1-\gamma_0)I_L \end{pmatrix} \cdot \delta\vec{\Gamma}_t. \tag{24}$$

The eigenvalues of the fundamental matrix

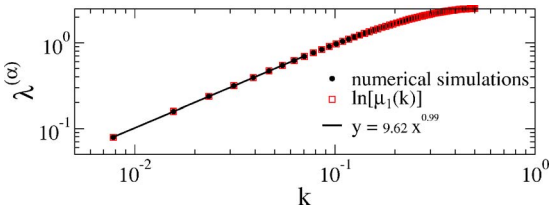

FIG. 19. (Color online) The dispersion relation $\lambda^{(\alpha)}$ vs. k for the model Eq. (8) with $f(z)=2z \pmod 1$ and $\epsilon=-1.3$. The agreement of the numerical simulations and the analytical estimation, which is $\lambda \equiv \ln[\mu_1(k)] = \ln[(\eta+2+\sqrt{\eta^2+4\eta})/2]$, is perfect.

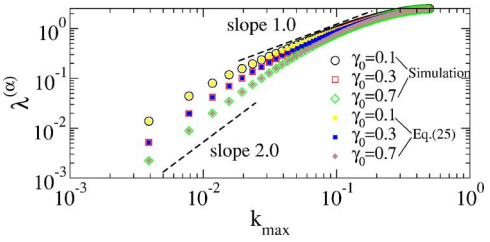

FIG. 20. (Color online) Dispersion relation $\lambda^{(\alpha)}$ vs. k for the model Eq. (8) with $f(z)=2z$ (mod 1) and $\gamma_t'=\gamma_0$. The open symbols represent the results of numerical simulations using Benettin's method while the filled symbols are for the analytical result stated in Eq. (25). The agreement between them is perfect. The parameter setting used is $L=256$ and $\epsilon=-1.3$.

$$\begin{pmatrix} I_L + 2\epsilon D_L & (1-\gamma_0)I_L \\ 2\epsilon D_L & (1-\gamma_0)I_L \end{pmatrix}$$

are

$$\mu_\pm = \frac{\eta + 2 - \gamma_0 \pm \sqrt{(\eta+2-\gamma_0)^2 - 4(1-\gamma_0)}}{2}, \qquad (25)$$

with $\eta=\eta(k)=-4\epsilon(1-\cos k)$. Again, the Lyapunov exponents are just $\lambda(k)\equiv\ln|\mu(k)|$. After some algebraic calculations, one finds for the positive branch $\lambda(k)=\ln|\mu_1(k)|$ and for $\epsilon<0$ that as $k\to 0$

$$\lambda(k) \simeq -\frac{2\epsilon}{\gamma_0}k^2, \qquad (26)$$

i.e., the dispersion relation for the model of Eq. (8) under damping switches to the universality class $\lambda\sim k^2$. The negative branch decreases quadratically starting with $\ln(1-\gamma_0)$ near $k\simeq 0$. Thus the Lyapunov spectrum also exhibits a gap at $k=0$. Note also that the result Eq. (26) implies that the dispersion relation for the limiting case $\gamma_0\to 0$ is different from the Hamiltonian case $\gamma_0=0$, i.e., the Lyapunov spectrum is a nonanalytic function of γ_0 near $\gamma_0=0$.

In numerical simulations, the system sizes used are always finite. This gives rise to a discrete lattice in k space; especially there exists a minimum wave number $k_0=2\pi/L$, which can be observed numerically. Therefore, due to this finite size effect the asymptotic scaling in Eq. (26) may not always be observable and some other regimes could be of interest as well (see Fig. 20). For example, for the case with $\gamma_0 \ll 1.0$, i.e., if the damping is quite weak,

$$\lambda(k) \simeq \sqrt{2|\epsilon|}k \qquad (27)$$

in the regime $1 \gg k \gg \sqrt{\gamma_0/2\epsilon}$. Therefore, for the case with $1 \gg \sqrt{\gamma_0/2\epsilon} \gg 2\pi/L$, there is a crossover in the dispersion relation from $\lambda^{(\alpha)}\sim k$ to $\lambda^{(\alpha)}\sim k^2$ with decreasing k. For the case with $k_0\equiv 2\pi/L > \sqrt{\gamma_0/2\epsilon}$, $\lambda^{(\alpha)}\sim k$ becomes the only observable nontrivial scaling regime.

The numerical simulations for the model Eq. (8) with $f(z)=2z$ (mod 1) and $\gamma_t'=\gamma_0\neq 0$ are presented in Fig. 20. As expected, for the cases with large damping, for instance with $\gamma_0=0.7$, there is $\lambda^{(\alpha)}\sim k^2$ as k approaches $2\pi/L$. Note, however, that for $\gamma_0=0.1$ this scaling regime is shifted to so small k values that it cannot be observed for such a system size. Instead one observes only the transition regime predicted in Eq. (27). All these simulations are in perfect agreement with our analytical results in Eqs. (26) and (27).

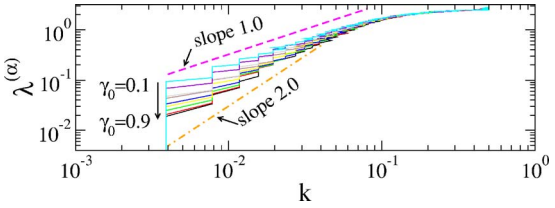

FIG. 21. (Color online) Dispersion relation $\lambda^{(\alpha)}$ vs. k for the coupled standard maps Eq. (8) with $\gamma_t'=\gamma_0\neq 0$. The results are similar to those shown in Fig. 20. This simulation confirms the validity of Eqs. (26) and (27) for more general systems beyond the one with $f(z)=2z$ (mod 1).

Simulations for the coupled standard maps Eq. (8) with $\gamma_0=0.1$ to 0.9 are shown in Fig. 21. Both scaling relations predicted by Eqs. (26) and (27) are observed. This supports the validity of these results for a general system beyond the one with $f(z)=2z$ (mod 1). Connected with the change in the dispersion relation, the propagating modes in a Hamiltonian system become stationary under damping. These facts will be described in detail in a separate publication [26] where the properties of the dynamic LV structure factors $S_u^{(\alpha\alpha)}(k,\omega)$ [see Eq. (7)] are explored.

X. RELATION BETWEEN THE MOMENTUM AND COORDINATE PART OF LVS

Remember that the LVs $\Gamma^{(\alpha)}$ of coupled standard maps are composed of two parts $\Gamma_u^{(\alpha)}=\{\delta u^{(\alpha)l}\}$ and $\Gamma_v^{(\alpha)}=\{\delta v^{(\alpha)l}\}$. In the above sections only the u component $\Gamma_u^{(\alpha)}$ was investigated. We now discuss also the v component $\Gamma_v^{(\alpha)}$.

In the study of hard-core systems [11], the angle between the two components $\Gamma_u^{(\alpha)}$ and $\Gamma_v^{(\alpha)}$ was investigated by considering

$$\cos\theta_{uv}^{(\alpha)} = \frac{\Gamma_u^{(\alpha)}\cdot\Gamma_v^{(\alpha)}}{|\Gamma_u^{(\alpha)}||\Gamma_v^{(\alpha)}|}. \qquad (28)$$

In Fig. 22, the values of $\cos\theta_{uv}^{(\alpha)}$ for coupled standard maps with $\epsilon=0.6$ are plotted versus the index α of LVs. One can see that $\cos\theta_{uv}^{(\alpha)}$ decreases gradually with increasing α. It

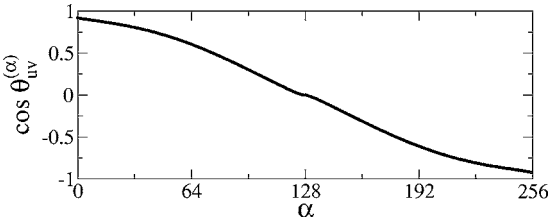

FIG. 22. $\cos\theta_{uv}^{(\alpha)}$ [see Eq. (28)] for the coupled standard maps Eq. (8) with $\epsilon=0.6$. From the plot one can infer that the u and v components of LVs with $\alpha\approx 128$, i.e., $\lambda^{(\alpha)}\approx 0$, are nearly orthogonal.

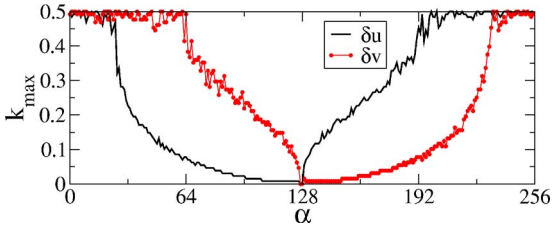

FIG. 23. (Color online) The peak wave number k_{max} vs. α for the u and v components of the LVs for the coupled standard maps Eq. (8) with $\epsilon=0.6$. The two curves are mutual mirror image due to the symmetry of Hamiltonian system $\Gamma_v^{(\alpha)}=-\Gamma_u^{(2L+1-\alpha)}$.

comes close to 1.0 as α goes to 1 which means that for those LVs associated with the largest LEs the two components are nearly parallel. While in the regime $\alpha \approx L$, where the HLMs are found in the u component of LVs, the absolute value of $\cos\theta_{uv}^{(\alpha)}$ is quite small. This implies that the two components for these LVs are nearly orthogonal. Therefore the study of the behavior of the v component is of equal importance as that of the u component.

An interesting feature of a LV $\Gamma^{(\alpha)}=\{\Gamma_u^{(\alpha)},\Gamma_v^{(\alpha)}\}$ of Hamiltonian systems is that $\Gamma_v^{(\alpha)}=-\Gamma_u^{(2L+1-\alpha)}$ [11,39]. This is confirmed by the symmetries borne by the quantities shown in Figs. 22–25. Owing to this symmetry, in the remaining part of this section we focus our attention on the part of LVs with $1 \leqslant \alpha \leqslant L$, which contains already the same amount of information as the total set of LVs.

The peak wave number k_{max} for the u and v components of LVs of the coupled standard maps with $\epsilon=0.6$ are presented in Fig. 23. It is obvious that the value of k_{max} for δv is larger than that for δu.

We define a quantity measuring the total spectral power in the u or v component of a Lyapunov vector,

$$S_{tot}^{(\alpha)} \equiv \int S_\zeta^{(\alpha\alpha)}(k)\mathrm{d}k = \sum_l |\delta\zeta^{(\alpha)l}|^2 \tag{29}$$

with $\zeta=u$ or v. Here $S_\zeta^{(\alpha\alpha)}(k)$ is the static LV structure factor. As can be seen in Fig. 24, for $\alpha<128$ corresponding to $\lambda^{(\alpha)}>0$ the total power in the v component of a LV is always smaller than in the u component. The two quantities attain their maximum/minimum value at $\alpha \simeq 115$. Since the LVs are all normalized unit vectors, the sum of the total power in

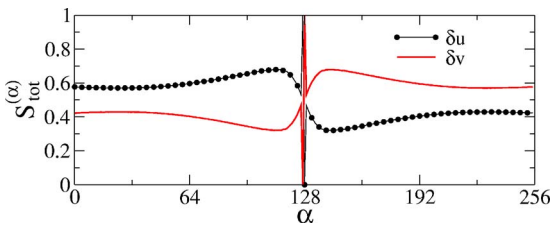

FIG. 24. (Color online) $S_{tot}^{(\alpha)}$ vs. α for the coupled standard maps Eq. (8) with $\epsilon=0.6$. Here $S_{tot}^{(\alpha)}$ [see Eq. (29)] is the total power in the u or v component of a LV with index α. For $\alpha<128$, i.e., $\lambda^{(\alpha)}>0$, the total power in the v component of a LV is always smaller than in the u component.

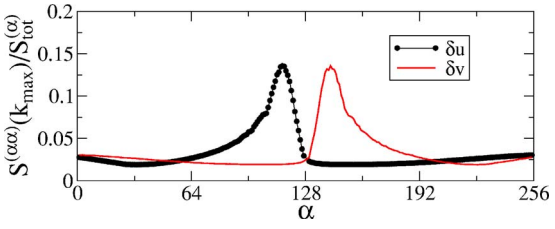

FIG. 25. (Color online) The normalized height $S^{(\alpha\alpha)}(k_{max})/S_{tot}^{(\alpha)}$ of the highest peak in the static LV structure factors of the coupled standard maps Eq. (8) with $\epsilon=0.6$. This quantity is a rough measure of the significance of the HLMs. Numerical results show that coherent wave structures are more significant in u components than in v components.

the two components is equal to 1 irrespective of the index α. This can be easily seen from Fig. 24.

The normalized height $S^{(\alpha\alpha)}(k_{max})/S_{tot}^{(\alpha)}$ of the highest peak in the static LV structure factor of a LV provides a rough estimation of the weight of the coherent long-wavelength structure contained in this LV. In other words, it is a measure of the significance of the HLMs. As can be seen in Fig. 25, the normalized height for the u component has a sharp peak at $\alpha \simeq 115$. In contrast, the curve of the normalized height for the v component is relatively flat and it attains a minimum value at the same place $\alpha \simeq 115$.

Before proceeding, we show some results about the force-like coupled Hamiltonian system Eq. (8) with $f(z)=2z \pmod 1$. The total power in the two components of LVs are presented in Fig. 26. As demonstrated in Fig. 27, there is a perfect agreement between the numerical results and analytical calculations of the quantity $c_1(k)$ [see Eq. (22)] in the considered regime $1 \leqslant \alpha \leqslant L$.

Now we provide a qualitative explanation of the observed difference in the u and v components of LVs of Hamiltonian systems. In analogy to Eqs. (13) and (14), the LV fluctuation densities for the u and v components can be written as

$$\mathcal{U}^{(\alpha)}(r,t) = \sum_k \mathcal{U}_k^{(\alpha)}(t)\exp(jkr), \tag{30a}$$

$$\mathcal{V}^{(\alpha)}(r,t) = \sum_k \mathcal{V}_k^{(\alpha)}(t)\exp(jkr). \tag{30b}$$

In Sec. IX it was shown that for $1 \leqslant \alpha \leqslant L$ the LVs are of the form $\{\vec{e}_l; c_1(k)\vec{e}_l\}$ if the nonlinear function $f(z)$

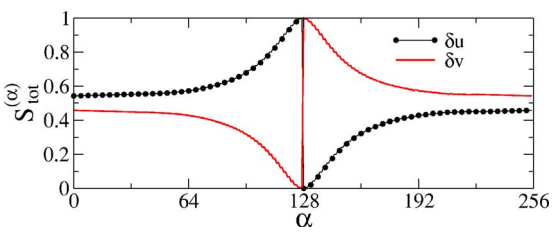

FIG. 26. (Color online) Similar to Fig. 24 but with $f(z)=2z \pmod 1$ and $\epsilon=-1.3$. Again for $\lambda^{(\alpha)}>0$ the total power in the v component of a LV is smaller than in the u component especially for the regime $\lambda^{(\alpha)} \approx 0$ where HLMs were found in the u component.

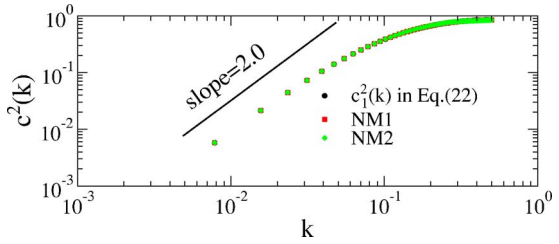

FIG. 27. (Color online) $c_1^2(k)$ vs. k for the force-like coupled Hamiltonian system Eq. (8) with $f(z)=2z$ (mod 1) and $\epsilon=-1.3$. The analytical result from Eq. (22) and the two numerical estimations, where NM1 is the ratio $S_v^{(\alpha\alpha)}(k_{max})/S_u^{(\alpha\alpha)}(k_{max})$ and NM2 is $\Sigma_l|\delta u^{(\alpha)l}|^2/\Sigma_l|\delta v^{l(\alpha)}|^2$, agree quite well.

$=(1/2\pi)\sin(2\pi z)$ in Eq. (8) is replaced by the Bernoulli shift map $f(z)=2z$ (mod 1). Here $\vec{e}_l$, which represent a set of plane waves, are the eigenvectors of the matrix D_L. For a general choice of $f(z)$, such as the nonlinear function $f(z)=(1/2\pi)\sin(2\pi z)$ used here, an intuitive picture of the LVs is that they are a mixture of the vectors $\{\vec{e}_l; c_1(k)\vec{e}_l\}$ with different weights. Then it is natural to expect that there is a relation

$$\mathcal{V}_k^{(\alpha)}(t) = c_1(k)\mathcal{U}_k^{(\alpha)}(t) \tag{31}$$

where the factor $c_1(k)$ is given in Eq. (22). A direct consequence of this relation is

$$S_v^{(\alpha\alpha)}(k) = c_1^2(k)S_u^{(\alpha\alpha)}(k), \tag{32}$$

which is checked by our numerical simulations. In Fig. 28, the ratios $S_v^{(\alpha\alpha)}(k)/S_u^{(\alpha\alpha)}(k)$ for several LVs of the coupled standard maps Eq. (8) with $\epsilon=0.6$ are shown. The value of $c_1^2(k)$ from Eq. (22) with $\epsilon=-0.6$ is plotted in the same figure. It can be seen that the estimated ratios follow the trend of $c_1^2(k)$ quite well especially in the regime $k \ll 1$. Since $c_1(k) \sim k$ as k approaches zero, following Eq. (32) we find $S_v^{(\alpha\alpha)}(k) \sim k^2 S_u^{(\alpha\alpha)}(k)$, which implies that the HLMs are weaker or even do not exist in the v component of LVs by the same reasons as discussed in connection with Eq. (17).

These facts demonstrate clearly that the momentum-like v component of a LV for the coupled Hamiltonian maps is related to its u counterpart (coordinate-like) but they have different properties. It is expected that these results are also

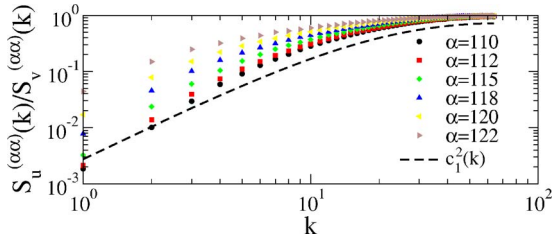

FIG. 28. (Color online) Ratios $S_v^{(\alpha\alpha)}(k)/S_u^{(\alpha\alpha)}(k)$ versus k for several LVs of coupled standard maps Eq. (8) with $\epsilon=0.6$. For comparison, the value of $c^2(k)$ for the case of coupled Bernoulli shift maps with $\epsilon=-0.6$ [see Eq. (22)] is plotted as a dashed line in the same figure. As $k \to 0$, the ratios follow the trend of $c_1^2(k) \sim k^2$ quite well.

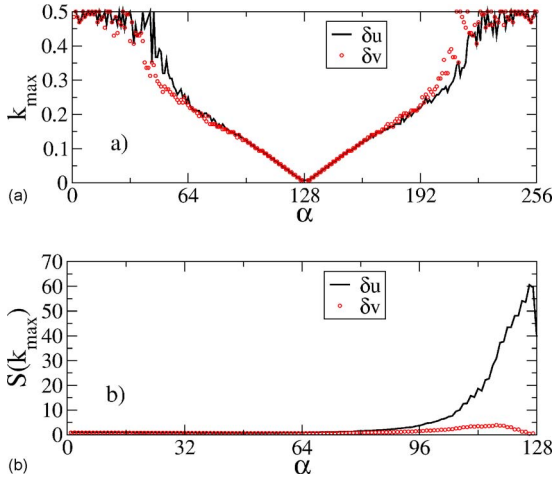

FIG. 29. (Color online) (a) Peak wave number k_{max} and (b) $S(k_{max})$ vs. α for the u and v components of LVs for the coupled skewed tent maps with $\epsilon=1.3$ and $r=0.2$ [40]. The coincidence of k_{max} for both components of LVs in the regime $\lambda \approx 0$ supports our statement that it is possible to observe the indication of HLMs in the momentum part of Lyapunov vectors if the HLMs in the corresponding coordinate part is significant enough. The comparision of $S(k_{max})$ for the parts of LVs shows that the long wavelength structures in the momentum part are much weaker than in the corresponding coordinate part.

valid for other Hamiltonian systems such as many-particle systems.

For the similar arguments as given in the final paragraph of Sec. V in connection with Eq. (17), we know from Eq. (32) that it is possible to observe similar long-wavelength structures in the momentum part of Lyapunov vectors, if the hydrodynamic Lyapunov modes in the coordinate parts are significant enough. One example case is presented in Fig. 29, where the nonlinear function $f(z)$ in Eq. (8) takes the form of skewed tent maps as used in Fig. 12. In view of the numerical results reported in Ref. [18], hard-core systems provide another example.

XI. ZERO-VALUE LYAPUNOV EXPONENTS AND ASSOCIATED LYAPUNOV VECTORS

As we have already mentioned, it is well known that continuous symmetries imply the existence of conservation laws for Lagrangian or Hamiltonian systems. The conserved quantities correspond to certain directions in tangent space along which perturbations grow slower than exponentially, i.e., the associated LEs are zero. It is also believed that these zero-value LEs and the corresponding LVs are the organizing center for the part of the Lyapunov spectrum around zero and HLMs. In this section we will see how the LEs and LVs associated with the conserved quantity and/or translational invariance behave in the model systems studied in the past sections.

As shown in Fig. 30, the LV nos. 128 and 129 for the force-like coupled standard maps are of the form $\delta u_t^l = c_0$, $\delta v_t^l = 0$ or $\delta v_t^l = c_0$, $\delta u_t^l = 0$. The LV no. 164 for the force-like coupled circle maps is $\delta u_t^l = c_0$. Here c_0 is a constant. The

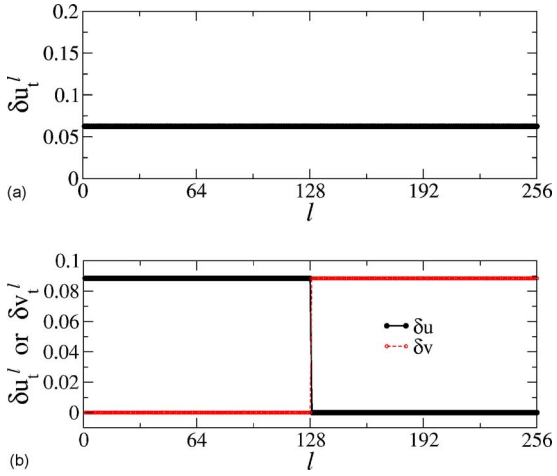

FIG. 30. (Color online) (a) Profile of u and v components of LV nos. 128 and 129 of coupled standard maps Eq. (8) and (b) that for LV no. 164 of coupled circle maps Eq. (10). The LVs shown are associated with translational invariance.

Lyapunov exponents associated with these LVs are of the order 10^{-19}, which can be regarded as identical to zero.

For the two models with translational invariance but without conserved quantity discussed in Sec. VI, the smallest absolute values of the LEs are of the order 10^{-6}. The profiles of the corresponding LVs are shown in Fig. 31.

The profile of the LV no. 164 for the diffusively coupled circle maps is shown in Fig. 32. The corresponding LE is of the order 10^{-6}.

One conclusion drawn from the above simulations is that the profiles of the LVs associated with zero-value LEs can be quite different. This difference is most obvious by comparing systems with translational invariance, which are distinguished by the existence or nonexistence of a conserved quantity.

It is also strange that in the two models with translational invariance but without conserved quantities [Eqs. (18) and (19)] the LVs associated with zero LEs are featureless. In the

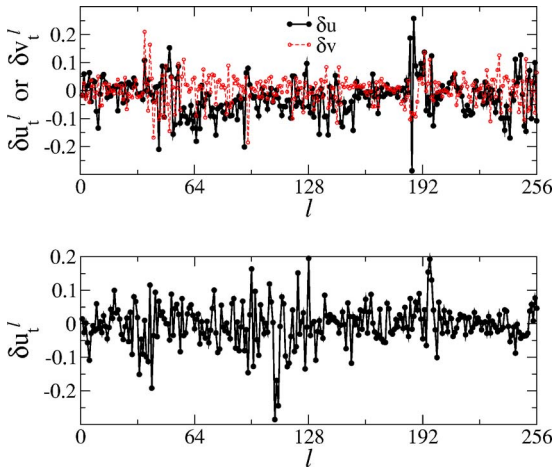

FIG. 31. (Color online) Similar to Fig. 30 but for the case with asymmetric interaction with $f(z)=(1/2\pi)\sin(2\pi z)$ and $g(z)=(1/2\pi)\cos(2\pi z)$ [cf. Eq. (18)]. Note in contrast to Fig. 30 the LVs associated with translational invariance are now featureless.

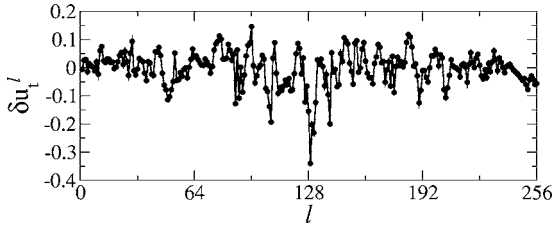

FIG. 32. Profile of LV no. 164 for the diffusively coupled circle maps with $\epsilon=1.3$ [see Eq. (11)]. This LV corresponds to the conservation law of the system considered.

study of hard-core systems, it is conjectured that the LV corresponding to space translational invariance is of the form (1,1,…,1;0,0…,0) or (0,0…,0;1,1,…,1). In analogy to this, we expected that for all the CMLs with translational invariance in u direction, the LVs associated with zero LEs should be of the form $\delta u_t^l=c_0$, $\delta v_t^l=0$ or $\delta v_t^l=c_0$, $\delta u_t^l=0$ as shown in Fig. 30. In this sense, the results shown in Fig. 31 for the models of Eqs. (18) and (19) are unexpected. Although it was not stated explicitly, it seems that the above conjecture about the structure of the LVs associated with zero-value LEs is based on the assumption that the numerically calculated Lyapunov vectors are the same as the eigenvectors of the fundamental matrix M, where the fundamental matrix governs the time evolution of the linear perturbations in the tangent space as $\delta X_t=M(t,0;X_0)\cdot\delta X_0$ [2]. The same assumptions are also made in the theoretical investigations of HLMs [10–13]. Our above numerical results show that the two sets of vectors are not identical in general.

Now we turn to another quantity which can provide complementary information about the Lyapunov instabilities of our systems. In contrast to the normal Lyapunov exponent which is the result of an average over an infinitely long period of time, the finite-time Lyapunov exponent $\lambda_\tau(t)$ characterizes the instabilities of trajectory segments of time duration τ centered at time t. The standard deviation $\sigma(\lambda_\tau)$ measures how strong the fluctuations of the local instabilities of the system are. Here we provide information for two cases, the force-like coupled standard maps and the diffusively coupled circle maps. Our emphasis is on showing the difference in the time fluctuations of the zero-value LEs of the two kinds of systems (Figs. 33 and 34). For the case of coupled standard maps, $\sigma(\lambda_\tau)$ for the zero-value LEs with $\alpha=127$ and 128 are of the order 10^{-16}, which is quite small in comparison to those of their neighbors, for example $\sigma(\lambda_\tau)\simeq 0.08$ for $\alpha=126$ and 129. However, for the case of diffusively coupled circle maps, $\sigma(\lambda_\tau)$ changes continuously with the index α and there is nothing special for the LE with $\alpha=164$. Here $\lambda^{(163)}=4.0\times10^{-4}$, $\lambda^{(165)}=-2.0\times10^{-4}$, and $\lambda^{(164)}=-4.0\times10^{-6}$. There is also no essential difference between the temporal evolution of the finite-time Lyapunov exponents λ_τ for $\alpha=163$ and for $\alpha=164$. Recalling that the zero-value LEs for the force-like coupled standard maps correspond to translational invariance while the one zero Lyapunov exponent in the diffusively coupled circle maps stems from the conservation law $Q_{t+1}=Q_t$, the differences in the time evolutions of the finite-time LEs and $\sigma(\lambda_\tau)$

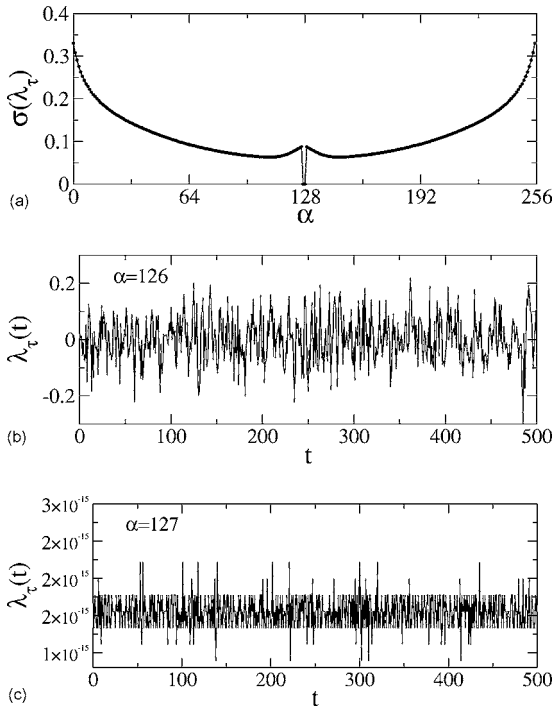

FIG. 33. (a) The fluctuations $\sigma(\lambda_\tau)$ vs. α show strong variation in the neighborhood of the zero LEs (α=127,128). This is demonstrated by the temporal evolution of the finite-time Lyapunov exponent λ_τ for α=126 and α=127. The results shown are for the force-like coupled standard maps Eq. (8) with ϵ=1.3.

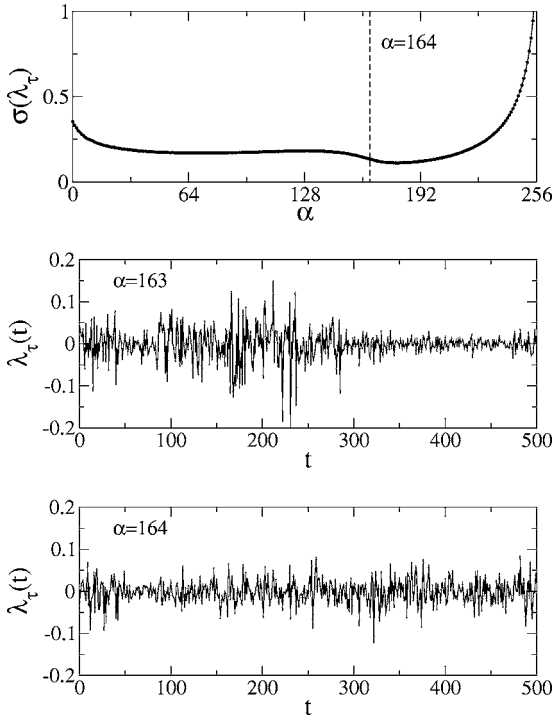

FIG. 34. Similar to Fig. 33 but for the diffusively coupled circle maps Eq. (11) with ϵ=1.3. Here the zero-value LE behaves quite similar to its nonzero neighbours.

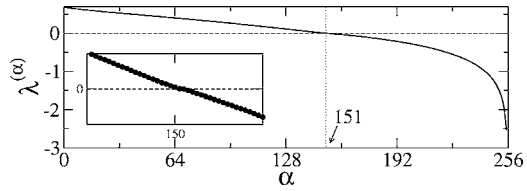

FIG. 35. Lyapunov spectrum for the force-like coupled circle maps on a two-dimensional 16×16 lattice with ϵ=0.8 [see Eq. (33)]. The inset shows the part about λ=0.

demonstrate once again that conservation laws and translational invariance play different roles in the tangent space dynamics.

XII. HLMS IN TWO-DIMENSIONAL CMLS

In previous studies, HLMs were already found in two- and three-dimensional hard-core systems [7] and in one- and two-dimensional soft-core systems [15–17]. Here, in order to demonstrate that the existence of HLMs in the systems of coupled map lattices is not restricted to the one-dimensional case, we show an example of two-dimensional CMLs. The system consists of force-like coupled circle maps on a square lattice. The equation of motion reads

$$u_{t+1}^{l,m} = u_t^{l,m} + \epsilon[f(u_t^{l+1,m} - u_t^{l,m}) + f(u_t^{l,m+1} - u_t^{l,m}) - f(u_t^{l,m} - u_t^{l-1,m}) - f(u_t^{l,m} - u_t^{l,m-1})], \quad (33)$$

where l and m are the indexes for the lattices sites and $f(z) = (1/2\pi)\sin(2\pi z)$. Periodic boundary conditions are imposed.

The Lyapunov spectrum of a 16×16 lattice with ϵ=0.8 is shown in Fig. 35. The zero-value LE is of the index α =151. Now the Lyapunov vectors become scalar fields on the two-dimensional lattice. The static LV structure factor, which is the spatial Fourier spectrum of the LV, is a scalar field on the two-dimensional reciprocal lattices in k space. Two examples for LV nos. 130 and 146 are shown in Fig. 36. The existence of sharp peaks in the spectra is obvious. The dispersion relations $\lambda^{(\alpha)}$ vs. $k_{max}^{(\alpha)}$ for the studied 16×16 lattice is shown in Fig. 37. The value of $k_{max}^{(\alpha)}$ decreases gradually as $\lambda^{(\alpha)}$ approaches zero. It implies that these LVs with $\lambda \simeq 0$ exhibit long-wavelength structures. Thus HLMs also exist for two-dimensional CMLs. Simulations for other cases with different parameters and/or lattice geometry yield similar results. From arguments as in Sec. IX, i.e., from systems with $f(z)=2z$ (mod 1), we expect a dispersion relation $\lambda \sim k^2$ for the HLMs in the d-dimensional lattice of dissipative maps. Results of numerical simulations have verified this conjecture for two-dimensional coupled circle maps (see Fig. 37).

Since in general $\alpha \sim k^d$ holds for a d-dimensional lattice model with HLMs, the corresponding λ-α relation becomes $\lambda \sim \alpha^{2/d}$. This implies that the Lyapunov spectrum in the regime $\lambda \approx 0$ has different shapes for each space dimension d. The Lyapunov spectrum in Fig. 35 shows that $\lambda \sim \alpha$ in the regime $\lambda \approx 0$ for the two-dimensional models, which is different from the relation $\lambda \sim \alpha^2$ for the one-dimensional case (see Fig. 5). In contrast, the uniform $\lambda \sim k^2$ dispersion rela-

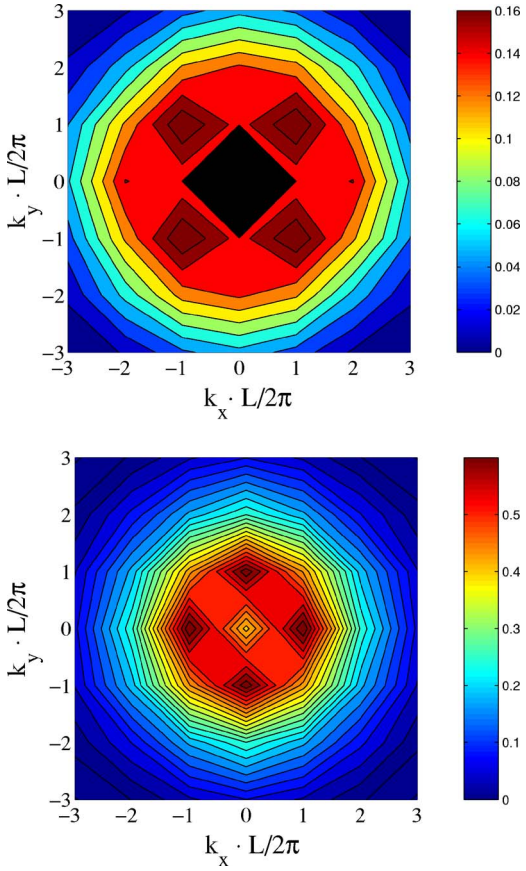

FIG. 36. (Color online) Contour plot of the static LV structure factor for LV nos. 130 and 146 of the force-like coupled circle maps on a two-dimensional 16×16 lattice with $\epsilon=0.8$. The existence of sharp peaks in the spectra is obvious.

tion demonstrates clearly the universal aspects of dissipative systems with continuous symmetries and conserved quantities.

XIII. DISCUSSION AND CONCLUSIONS

Through the series of numerical experiments performed we come to the following conclusions: (1) HLMs do exist in CMLs with continuous symmetries. To our knowledge, this is the first time HLMs are reported for such systems. (2) The finding of HLMs in a system of coupled dissipative maps shows that the Hamiltonian structure is not necessary for the appearance of the HLMs. (3) The λ-k dispersion relations of HLMs belong to two universality classes. The one for the coupled standard maps is $\lambda\sim k$ while the other for the coupled circle maps is $\lambda\sim k^2$. (4) Conservation laws and translational invariance are crucial for the appearance of HLMs but either one alone cannot guarantee the appearance of HLMs. (5) Damping in the system of coupled standard maps will not destroy the HLMs. However, the dispersion relation changes to $\lambda\sim k^2$ under damping. (6) Addition of an on-site potential destroys the HLMs. (7) The momentum part of LVs behaves differently from the coordinate part but they are related.

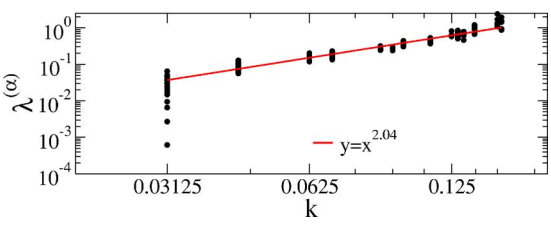

FIG. 37. (Color online) Dispersion relation $\lambda^{(\alpha)}$ vs. k_{max} of the force-like coupled circle maps on a two-dimensional 32×32 lattice with $\epsilon=2.0$. Fitting the numerical data to a power-law $\lambda^{(\alpha)}\sim k_{max}^{\beta}$ yields $\beta\simeq2.04$, i.e., the two-dimensional lattice of dissipative maps is also characterized by a quadratic dispersion relation as the one-dimensional case shown in Fig. 17.

All these results are obtained for force-like coupled maps. For diffusively coupled maps the situation is less clear. In our studies we found cases where HLMs appear to exist, but there are other cases where they cannot be found. We are able to explain this in connection with associated force-like coupled maps, but the full understanding has not been achieved.

It is appropriate to recall a closely related work by Eckmann and Gat [10]. They proposed a random matrix model for the tangent space dynamics of translational invariant systems and proved that HLMs exist in this class of system if the fundamental matrix of the tangent dynamics is subject to the constraint of uniform hyperbolicity. As they stated, the tangent dynamics they proposed is similar to that of an anharmonic chain like the FPU model except that the fundamental matrix of the FPU model is elliptic rather than hyperbolic as they assumed. The tangent space dynamics of the CMLs studied here can be similar to either the case of the FPU model or that proposed by Eckmann and Gat, depending on the form of the nonlinear function $f(z)$ used. For instance, if $f(z)$ takes the form of a skewed Bernoulli shift map [45], the tangent dynamics of CMLs is uniformly hyperbolic akin to the model proposed by Eckmann and Gat while the tangent dynamics is similar to that of the FPU model for $f(z)=(1/2\pi)\sin(2\pi z)$. Our numerical experiments imply that some of the strong assumptions, e.g., uniform hyperbolicity, used in the proof of Eckmann and Gat can be relaxed. Further work in this direction is undertaken and will be presented elsewhere.

One important finding of the current study is that the dispersion relations for HLMs belong to different universality classes. It seems that the previously studied many-particle systems like the hard-core system and the Lennard-Jones system are in the same universality class as the coupled standard maps. Our finding of the change of the universality class for coupled Hamiltonian maps under damping, especially the case with time-dependent damping, suggests that it is possible that the nonequilibrium cases of color conduction studied by Posch *et al.* are in the universality class $\lambda\sim k^2$. It seems that a Hamiltonian structure is needed for obtaining a linear dispersion relation, while already small dissipative terms change the dispersion relation to a quadratic form. Actually the dispersion relation is not the only difference between the two classes, our simulations show that the HLMs in coupled circle maps are nonpropagating while the modes in coupled standard maps are indeed propagating. Details

about the dynamics of the HLMs will be presented elsewhere [26].

In the literature, there are already many studies on the universal shape of Lyapunov spectra in the thermodynamic limit [42], where an universal linear relation $\lambda \sim \alpha$ in the regime $\lambda \approx 0$ has been suggested for a certain class of systems. For most systems treated in the current work, the constraint of continuous symmetries and conserved quantities leads to some essential changes in the tangent space dynamics. First of all, the constraint guarantees the existence of HLMs, i.e., the long-wavelength structures in the Lyapunov vectors associated with near-zero Lyapunov exponents. In view of this, the λ-k dispersion relation contains additional information about the wave-like characteristics of Lyapunov vectors compared to the λ-α relation, even though they take identical forms in the one-dimensional systems. Second, under the influence of continuous symmetries and conserved quantities, there are changes in the λ-α relation. For instance, a quadratic relation $\lambda \sim \alpha^2$ is observed for the one-dimensional dissipative systems. The resultant condensation of Lyapunov exponents at $\lambda \approx 0$ can be easily observed in Fig. 5 and 14. Finally, after going to high-dimensional spaces, the λ-k dispersion relation remains invariant while the λ-α relation varies with the lattice dimension d (see Sec. XII for the case of two-dimensional lattice of circle maps). All these facts demonstrate clearly the differences between the current work and the previous studies [42].

In the early stage of the study on HLMs in hard-core systems, only the coordinate part of the Lyapunov vectors was considered, which is based on the numerical observation that the momentum part of the Lyapunov vectors is nearly parallel (or anti-parallel) to the corresponding coordinate part if the associated Lyapunov exponents are close to zero [9,11]. Later numerical simulations for both the hard-core systems [13] and the Lennard-Jones fluids [15] show that this is in general not the case. Although there have already been some investigations about both parts of the Lyapunov vectors, a systematic investigation of the relation between them is lacking until now. Our arguments in Sec. X in the light of the analytical treatment of a particular case serves to fill such a gap. Since the CMLs used here bear similar symmetries as the many-particle systems treated previously, it is anticipated that our arguments for the relation between the two parts of Lyapunov vectors could be valid for, or at least provide hints to, general extended systems with continuous symmetries, including the many-particle ones.

As we mentioned already in the above descriptions, there is a difference between the CMLs studied here and the many-particle systems investigated previously. For many-particle systems, the elements (particles) are located in the real physical space and the system dynamics takes place in the same space, i.e., the movement of the particles is also in the real physical space. For CMLs the elements are arranged on a discrete lattice while the system dynamics is continuous. If we denote the space where the elements are located (or embedded) as the *coordinate space* and refer to the space in which the dynamical evolution of the system takes place as the *state space* of the system, the coordinate and state space are different for CMLs while they are identical for many-particle systems. Careful studies are needed to get a complete understanding of the influence of this difference in the behavior of HLMs. Here we give just an example: In many-particle systems the HLMs corresponding to space translational invariance were classified into the transverse and longitudinal modes, respectively. For the CMLs studied in the current paper, such a classification of the HLMs no longer works. The situation is rather clear for the two-dimensional case studied in Sec. XII, only one sort of HLMs exists there.

One important open question in the study of HLMs is the relation between the continuous symmetries of the system and the HLMs. In the study of hard-core systems, three different kinds of HLMs are proposed [14]. The transverse and longitudinal modes are associated with the space translational invariance of the system and P modes (or time modes) result from the time-translational invariance of the system. The models considered in this paper do not obey continuous time translational invariance. This is most obvious for the coupled standard maps, which can be considered as the return map of a periodically kicked system in continuous time [35]. This implies that no zero mode is associated with this symmetry, hence this seems to be the reason for the absence of P modes in the CMLs considered.

It is generally accepted that the conserved quantities and the associated zero-value LEs are the organizing center of HLMs. In Sec. XI we found that there are two kinds of zero-value LEs. The zero-value LE in the force-like coupled circle maps is an example for the first kind. It is associated with the space translational invariance of the system dynamics. Here the absolute value of the LE is absolutely zero and there are nearly no fluctuations in the corresponding finite-time Lyapunov exponents. The associated Lyapunov vector is a uniform vector with equal values for all the components. The zero-value LE in the system of diffusively coupled circle maps is of the second kind. Here the LE is associated with an energy-like conserved quantity. It is only nearly equal to zero and there are large fluctuations in the finite-time Lyapunov exponents. The corresponding LV is featureless. The LEs associated with momentum conservation and the space translational invariance in many-particle systems are of the first kind while those due to the energy conservation and the time translational invariance are of the second kind. Further work is needed to investigate the difference in the associated HLMs.

ACKNOWLEDGMENTS

We acknowledge financial support from the Deutsche Forschungsgemeinschaft within SFB393 "Parallele Numerische Simulation für Physik und Kontinuumsmechanik."

[1] N. S. Krylov, *Works on the Foundations of Statistical Mechanics* (Princeton University Press, Princeton, 1979).
[2] P. Gaspard, *Chaos, Scattering, and Statistical Mechanics* (Cambridge University Press, Cambridge, 1998).
[3] J. P. Dorfman, *An Introduction to Chaos in Nonequilibrium Statistical Mechanics* (Cambridge University Press, Cambridge, 1999).
[4] D. J. Evans and G. P. Morriss, *Statistical Mechanics of Nonequilibrium Liquids* (Academic, New York, 1990).
[5] Wm. G. Hoover, *Computational Statistical Mechanics* (Elsevier, New York, 1991).
[6] Wm. G. Hoover, *Time Reversibility, Computer Simulation, and Chaos* (World Scientific, Singapore, 1999).
[7] H. A. Posch and R. Hirschl, "Simulation of Billiards and of Hard-Body Fluids," in *Hard Ball Systems and the Lorentz Gas*, edited by D. Szasz, Encyclopedia of the Mathematical Sciences, Vol. 101, p. 269 (Springer Verlag, Berlin, 2000).
[8] H. A. Posch and Ch. Forster, in *Collective Dynamics of Nonlinear and Disordered Systems*, edited by G. Radons, W. Just, and P. Häussler (Springer, Berlin, 2005), p. 309.
[9] C. Forster, R. Hirschl, H. A. Posch, and Wm. G. Hoover, Physica D **187**, 294 (2004).
[10] J.-P. Eckmann and O. Gat, J. Stat. Phys. **98**, 775 (2000).
[11] S. McNamara and M. Mareschal, Phys. Rev. E **64**, 051103 (2001); M. Mareschal and S. McNamara, Physica D **187**, 311 (2004).
[12] A. S. de Wijn and H. van Beijeren, Phys. Rev. E **70**, 016207 (2004).
[13] T. Taniguchi and G. P. Morriss, Phys. Rev. E **65**, 056202 (2002); **68**, 026218 (2003); **68**, 046203 (2003).
[14] J.-P. Eckmann, C. Forster, H. A. Posch, and E. Zabey, J. Stat. Phys. **118**, 813 (2005); see also arXiv: nlin.CD/0404007.
[15] H. L. Yang and G. Radons, Phys. Rev. E **71**, 036211 (2005), see also arXiv: nlin.CD/0404027.
[16] G. Radons and H. L. Yang, arXiv: nlin.CD/0404028.
[17] C. Forster and H. A. Posch, New J. Phys. **7**, 32 (2005), see also arXiv: nlin.CD/0404019.
[18] T. Taniguchi and G. P. Morriss, Phys. Rev. E **71**, 016218 (2005); Phys. Rev. Lett. **94**, 154101 (2005).
[19] K. Kaneko, Prog. Theor. Phys. **72**, 480 (1984); K. Kaneko, "Simulating Physic in Coupled Map Lattices," in *Formation, Dynamics, and Statistics of Patterns*, Vol. 1, edited by K. Kawasaki, A. Onuki, and M. Suzuki (World Scientific, Singapore, 1990).
[20] See the special issue on Coupled Map Lattices, Chaos **2**, 279–460 (1992).
[21] R. Tenny, L. S. Tsimring, L. Larson, and H. D. I. Abarbanel, Phys. Rev. Lett. **90**, 047903 (2003); T. Bohr, M. van Hecke, R. Mikkelsen, and M. Ipsen, *ibid.* **86**, 5482 (2001); F. Ginelli, R. Livi, A. Politi, and A. Torcini, Phys. Rev. E **67**, 046217 (2003); O. Rudzick and A. Pikovsky, *ibid.* **54**, 5107 (1996); H. L. Yang and E. J. Ding, *ibid.* **50**, R3295 (1994).
[22] See for example T. Bohr, G. Grinstein, and C. Jayaprakash, Chaos **5**, 412 (1995).
[23] Y. Pomeau, A. Pumir, and P. Pelce, J. Stat. Phys. **37**, 39 (1984); K. Kaneko, Physica D **23**, 436 (1986).
[24] G. Giacomelli and A. Politi, Europhys. Lett. **15**, 387 (1991).
[25] A. Pikovsky and A. Politi, Nonlinearity **11**, 1049 (1998); Phys. Rev. E **63**, 036207 (2001).
[26] H. L. Yang and G. Radons (unpublished).
[27] J. P. Boon and S. Yip, *Molecular Hydrodynamics* (McGraw-Hill, New York, 1980).
[28] For the case of many-particle systems including the hard-core and the Lennard-Jones systems, the physical space where the particles are located is identical to the state space of the particles, i.e., $\delta u_l^{(\alpha)}(t)$ is the perturbation on the coordinate $r_l(t)$. It is also possible that the physical space is different from the state space. The CMLs studied here provide an example: the physical space where the elements of the system are embedded is a discrete lattice, while the state space of the elements is a continuous one. For this case the position coordinate of the lth element $r_l=la$ is fixed and $\delta u_l^{(\alpha)}(t)$ is the perturbation on this element's state variable $u_l(t)$.
[29] V. I. Oseledec, Trans. Mosc. Math. Soc. **19**, 197 (1968).
[30] R. A. Johnson, K. J. Palmer, and G. R. Sell, SIAM J. Math. Anal. **18**, 1 (1987).
[31] I. Goldhirsch, P. L. Sulem, and S. A. Orszag, Physica D **27**, 331 (1987).
[32] S. V. Ershov and A. B. Potapov, Physica D **118**, 167 (1998).
[33] G. Benettin, L. Galgani, and J. M. Strelcyn, Phys. Rev. A **14**, 2338 (1976).
[34] I. Shimada and T. Nagashima, Prog. Theor. Phys. **61**, 1605 (1979).
[35] K. Kaneko and T. Konishi, Phys. Rev. A **40**, R6130 (1989).
[36] The extended nature of the Lyapunov vectors with near-zero Lyapunov exponents does not imply the existence of the hydrodynamic Lyapunov modes (HLMs). It is a more general property of the extended system than the HLMs.
[37] M. S. Bourzutschky and M. C. Cross, Chaos **2**, 173 (1992).
[38] R. Livi, M. Pettini, S. Ruffo, M. Sparpaglione, and A. Vulpiani, Phys. Rev. A **31**, 1039 (1985).
[39] U. Dressler, Phys. Rev. A **38**, 2103 (1988); G. P. Morriss and C. P. Dettmann, Chaos **8**, 321 (1998).
[40] The skewed tent map takes the form
$$f(z)=\begin{cases} rz & \text{for } 0 \leqslant z < 1/r, \\ \dfrac{r-rz}{r-1} & \text{for } 1/r \leqslant z < 1. \end{cases}$$
[41] E. Noether, "Invariante Varlationsprobleme," Nachr. d. König. Gesellsch. d. Wiss. zu Göttingen, Math-phys. Klasse (1918), pp. 235–257; English translation M. A. Travel, Transp. Theory Stat. Phys. **1**, 183 (1971).
[42] C. M. Newman, Commun. Math. Phys. **103**, 121 (1986); R. Livi, A. Politi, S. Ruffo, and A. Vulpiani, J. Stat. Phys. **46**, 147 (1987); J.-P. Eckmann and C. E. Wayne, J. Stat. Phys. **50**, 853 (1988); Y. Yamaguchi, J. Phys. A **31**, 195 (1998).
[43] The two constants a_1 and a_2 can be chosen properly to satisfy the normalization of the Lyapunov vectors. For simplicity, we will not consider the normalization of Lyapunov vectors in this section.
[44] For the case with $\epsilon>0$, there is a large group of Lyapunov exponents that are zero. The corresponding LVs are plane waves with $-k_0<k<k_0$. Thus there are no HLMs for this case.
[45] The skewed Bernoulli shift map takes the form
$$f(z)=\begin{cases} rz & \text{for } 0 \leqslant z < 1/r, \\ \dfrac{rz-1}{r-1} & \text{for } 1/r \leqslant z < 1. \end{cases}$$